Optimal energy conserving local discontinuous Galerkin methods for second-order wave equation in heterogeneous media

Ching-Shan Chou[1], Chi-Wang Shu[2] and Yulong Xing[3]

Abstract

Solving wave propagation problems within heterogeneous media has been of great interest and has a wide range of applications in physics and engineering. The design of numerical methods for such general wave propagation problems is challenging because the energy conserving property has to be incorporated in the numerical algorithms in order to minimize the phase or shape errors after long time integration. In this paper, we focus on multi-dimensional wave problems and consider linear second-order wave equation in heterogeneous media. We develop and analyze an LDG method, in which numerical fluxes are carefully designed to maintain the energy preserving property and accuracy. Compatible high order energy conserving time integrators are also proposed. The optimal error estimates and the energy conserving property are proved for the semi-discrete methods. Our numerical experiments demonstrate optimal rates of convergence, and show that the errors of the numerical solutions do not grow significantly in time due to the energy conserving property.

Keywords: wave propagation, local discontinuous Galerkin method, energy conservation, optimal error estimate, heterogeneous media

[1]Department of Mathematics, The Ohio State University, Columbus, OH 43221. Email: chou@math.ohio-state.edu. Research is supported by NSF grants DMS-1020625 and DMS-1253481.

[2]Division of Applied Mathematics, Brown University, Providence, RI 02912. E-mail: shu@dam.brown.edu. Research is supported by DOE grant DE-FG02-08ER25863 and NSF grant DMS-1112700.

[3]Computer Science and Mathematics Division, Oak Ridge National Laboratory, Oak Ridge, TN 37831 and Department of Mathematics, University of Tennessee, Knoxville, TN 37996. E-mail: xingy@math.utk.edu. Fax: (865) 241-4811. Research is sponsored by NSF grant DMS-1216454, ORNL and the U. S. Department of Energy, Office of Advanced Scientific Computing Research. The work was partially performed at ORNL, which is managed by UT-Battelle, LLC, under Contract No. DE-AC05-00OR22725.

1 Introduction

Wave propagation is a fundamental form of energy transmission, which arises in many fields of science, engineering and industry, and it is significant to geoscience, petroleum engineering, telecommunication, and the defense industry (see [24, 33] and the references therein). Efficient and accurate numerical methods to solve wave propagation problems are of fundamental importance to these applications. Experience reveals that energy conserving numerical methods, which conserve the discrete approximation of the energy, are favorable because they are able to maintain the phase and shape of the waves accurately, especially for long time simulation. In [44], we have designed a high order accurate energy conserving local discontinuous Galerkin (LDG) method for the one-dimensional second-order wave equation with constant coefficient. In this paper, we focus on multi-dimensional problems in heterogeneous media, and develop optimally convergent LDG methods which also conserve the energy in the discrete sense.

The wave equation can be written in a second-order form, or an equivalent first-order hyperbolic system. Directly solving the second-order equation usually involves fewer unknown variables, therefore the resulting numerical schemes are more efficient. This saving can be significant in the three-dimensional applications. For example, for the linear elasticity equations in three dimensions, three variables are used in the second-order form, while first-order system needs at least nine components [6]. In addition, there are many applications where the second-order PDEs arise naturally. When converted into first-order systems, they may admit a wider class of solutions, therefore some constraints are needed to ensure these solutions are solutions of the original second-order equation, which also increases difficulty to the design of numerical methods. Finally, it was also shown [3] that second-order equation may allow larger time step size, compared to the first-order system.

A vast amount of literature can be found on the numerical approximations of the second-order wave equation. The most common numerical method for solving the wave equation is to use the second order accurate centered finite difference operator. One major component

in designing such finite difference methods which conserve the energy numerically is the Summation By Parts (SBP) operator, with special attention paid near the boundaries. There have been many studies on this subject (see [43] and the references therein). While finite difference methods provide efficient solvers, they are largely limited by the geometry of the domain, although some attempts [4] have been made to circumvent this difficulty. In contrast, finite element methods have the flexibility in handling complex geometry. Safjan and Oden [41] introduced a family of unconditionally stable high order Taylor-Galerkin schemes for acoustic and elastic wave propagation. Faccioli et al. [25] used explicit Fourier-Legendre domain decomposition methods and focused on the numerical validation of the methods. Spectral methods for acoustic and elastic waves have been developed in [36, 46], and a mortar coupling between spectral and finite elements methods for elastodynamic problem on complex geometries can be found in [9]. Spectral element methods are shown to conserve energy when applied to the wave equations [2, 28]. We refer to [29, 20] for a review of previous work on spectral and spectral element methods. Here, we will confine our attention in discontinuous Galerkin (DG) methods, which have the advantages of being local (versus global), easy *h*-*p* adaptivity and being able to handle hanging nodes, compared with spectral element methods. DG methods can be viewed as spectral element methods with domain decomposition. They belong to a class of finite element methods using discontinuous piecewise polynomial spaces for both the numerical solution and the test functions. They were originally devised to solve hyperbolic conservation laws with only first order spatial derivatives, e.g. [14, 15, 16, 18, 19]. They allow arbitrarily unstructured meshes, and have compact stencils. Moreover, they easily accommodate arbitrary *h*-*p* adaptivity. DG methods were later generalized to the LDG methods by Cockburn and Shu to solve convection-diffusion equations [17], motivated by successful numerical experiments from Bassi and Rebay [7] for the compressible Navier-Stokes equations. Recently, Zhong and Shu [47] studied the question of how many grid points (degrees of freedom) per wave length are needed to achieve a given accuracy for the DG method applied to the linear wave equation, following the classical error analysis by

Kreiss and Oliger [35] for the finite difference methods.

Many DG methods have been developed for the wave equation in both first-order and second-order forms [16, 31, 26, 38, 41, 40, 1, 5], and some of these methods are also energy-conserving [27, 30, 12]. Two approaches are commonly used to achieve the energy-conserving property. The first one is to introduce two staggered mesh sets, and define one set of solution on each mesh. This usually leads to more complexity, as staggered mesh may be difficult to construct, especially for high dimensional complex domain and in the neighborhood of the boundary. Recently, Chung and Engquist [12, 13] have proposed an optimal, energy conserving DG method for the first-order wave equation using staggered grids. They introduced different meshes for different computational variables, and are able to prove the optimal convergence for unstructured meshes. The other approach to obtain energy-conserving method is to use the central numerical flux [27], i.e., the numerical flux along cell boundaries is evaluated by taking the average of two values of the numerical solution from the two neighboring cells. However, only suboptimal convergence can be proven theoretically, and numerically, one can observe optimal convergence if even order polynomial space is used, and suboptimal if odd order polynomial space is used.

Usually it is difficult to obtain DG schemes for wave equations which are non-dissipative (energy conserving for the physical energy) and optimal high order accurate. In [44], we have designed an energy conserving LDG method for the simple one-dimensional second-order constant coefficient wave equation. We have proved that the proposed method has the optimal convergence rates in both the energy and L^2 norms, and the upper bound of the errors grows in time only in a linear fashion. In this paper, we consider the multi-dimensional wave problems in heterogeneous media. Extension of the previous work to the multi-dimensional problems on Cartesian meshes is discussed. Extra attention needs to be paid at the interface of different media to ensure the stability and energy conservation. Theoretical proof, as well as the numerical evidence, indicates that a good choice of the projection of the initial condition into the polynomial space is important to achieve optimal convergence rate. The

semi-discrete LDG method will be coupled with high order explicit energy conserving time discretization. We remark here that since our scheme is non-dissipative, it is more oscillatory than the commonly used upwind (energy-dissipative) DG method when applied to problems with discontinuities. The advantage of energy-conserving methods is to solve smooth wave problems, with the attempt to resolve all waves for long time periods.

The outline of our paper is as follows. In Section 2, we present the semi-discrete LDG method, and prove its energy conserving property. The optimal error estimates, both in the energy norm and the L^2 norm, are analyzed in Section 3, and therein, the upper bound of errors is proved to grow linearly in time. The fully discrete LDG method, with the high order energy conserving time discretization, and its energy conserving properties are presented in Section 4. Section 5 contains numerical experiments that demonstrate the optimal convergence rates and energy conservation of the proposed LDG method, as well as its excellent long time accuracy. Finally, we give concluding remarks in Section 6.

2 Local discontinuous Galerkin discretization

2.1 The model problem

In this paper, we primarily consider the second-order wave equation, on a bounded domain Ω in $\mathcal{R}^2$ or $\mathcal{R}^3$,

$$u_{tt} = \nabla \cdot (a^2(\boldsymbol{x})\nabla u), \qquad \boldsymbol{x} \in \Omega, \quad t \in [0, T], \tag{2.1}$$

where $a(\boldsymbol{x}) > 0$, and this problem is subject to the initial conditions

$$u(\boldsymbol{x}, 0) = u_0(\boldsymbol{x}), \qquad u_t(\boldsymbol{x}, 0) = v_0(\boldsymbol{x}). \tag{2.2}$$

The speed of wave propagation is $a(\boldsymbol{x})$, which is assumed to be piecewise smooth. Both homogeneous Dirichlet boundary conditions and periodic boundary conditions will be considered. We remark here that the results in the following sections will remain the same if a source term $f(\boldsymbol{x}, t)$ is added to the equation (2.1), so for simplicity, we only consider (2.1) throughout this paper.

2.2 Notations

We consider a two-dimensional rectangular domain Ω for simplicity (extension to three dimension is straightforward), and without loss of generality, we denote it by $[0, L_x] \times [0, L_y]$. We discretize the computational domain Ω into rectangular cells $K_{i,j} = I_i \times J_j$, where $I_i = [x_{i-\frac{1}{2}}, x_{i+\frac{1}{2}}]$, $i = 1, \cdots, N_x$ and $J_j = [y_{j-\frac{1}{2}}, y_{j+\frac{1}{2}}]$, $j = 1, \cdots, N_y$. The center of each cell is $(x_i, y_j) = \left(\frac{1}{2}(x_{i-\frac{1}{2}} + x_{i+\frac{1}{2}}), \frac{1}{2}(y_{j-\frac{1}{2}} + y_{j+\frac{1}{2}})\right)$, and the mesh sizes are denoted by $h_i^x = x_{i+\frac{1}{2}} - x_{i-\frac{1}{2}}$ and $h_j^y = y_{j+\frac{1}{2}} - y_{j-\frac{1}{2}}$, with $h^x = \max_{1\le i\le N_x} h_i^x$, $h^y = \max_{1\le j\le N_y} h_j^y$, and $h = \max(h^x, h^y)$ the maximal mesh size. Regular meshes are used, namely, the ratio between the maximal and the minimal mesh sizes remains bounded during mesh refinement. Let $\mathcal{T}_h$ be the family of partitions of Ω parameterized by $h > 0$, and we define

$$\begin{aligned}
\mathcal{E}_h^I &:= \text{ set of all interior edges/faces of } \mathcal{T}_h, \\
\mathcal{E}_h^B &:= \text{ set of all boundary edges/faces of } \mathcal{T}_h \text{ on } \Gamma = \partial\Omega, \\
\mathcal{E}_h &:= \mathcal{E}_h^I \cup \mathcal{E}_h^B.
\end{aligned}$$

The piecewise polynomial space V_h^k is defined as the space of tensor products of piecewise polynomials of degree at most k in each variable on every element $K_{i,j}$, that is,

$$V_h^k = \{v : v|_K \in Q^k(K),\ \forall K \in \mathcal{T}_h\}, \tag{2.3}$$

where Q^k is the space of tensor products of one-dimensional polynomials of degree up to k. Note that functions in V_h^k are allowed to have discontinuities across element interfaces. We extend this definition to vector-valued functions by defining

$$\Sigma_h^k = \{\mathbf{w} = (w_1, w_2)^T : w_l|_K \in Q^k(K),\ l = 1, 2,\ \forall K \in \mathcal{T}_h\}. \tag{2.4}$$

The solution of the numerical scheme is denoted by u_h, which belongs to the finite element space V_h^k. We denote by $u_h(x_{i+1/2}^+, y)$ and $u_h(x_{i+1/2}^-, y)$ the limit values of u_h at $x_{i+\frac{1}{2}}$ from the right cell $I_{i+1} \times J_j$ and from the left cell $I_i \times J_j$, respectively; $u_h(x, y_{j+1/2}^+)$ and $u_h(x, y_{j+1/2}^-)$ are defined similarly. The L^2 norm over the domain Ω is denoted by $\|\cdot\|$.

2.3 The LDG method

In this subsection, we define the semi-discrete LDG method for the wave equation (2.1), by discretizing the space with the LDG method and leaving the time dependence continuous. The wave equation is written into a first order system by substituting the first order derivatives u_x, u_y with the auxiliary variable $\boldsymbol{q} = (q^1, q^2)$:

$$\begin{aligned} u_{tt} &= \nabla \cdot (a(\boldsymbol{x})\boldsymbol{q}), \\ \boldsymbol{q} &= a(\boldsymbol{x})\nabla u. \end{aligned} \tag{2.5}$$

The LDG method for (2.5) is then formulated as follows: find u_h, q_h^1, $q_h^2 \in V_h^k$, such that

$$\begin{aligned} \int_{K_{i,j}} (u_h)_{tt}\psi d\boldsymbol{x} + \int_{K_{i,j}} aq_h^1\psi_x d\boldsymbol{x} - \int_{J_j} \widehat{aq_h^1}\psi(x^-_{i+\frac{1}{2}}, y)dy + \int_{J_j} \widehat{aq_h^1}\psi(x^+_{i-\frac{1}{2}}, y)dy \\ + \int_{K_{i,j}} aq_h^2\psi_y d\boldsymbol{x} - \int_{I_i} \widetilde{aq_h^2}\psi(x, y^-_{j+\frac{1}{2}})dx + \int_{I_i} \widetilde{aq_h^2}\psi(x, y^+_{j-\frac{1}{2}})dx &= 0, \end{aligned} \tag{2.6}$$

$$\int_{K_{i,j}} q_h^1\phi d\boldsymbol{x} + \int_{K_{i,j}} au_h\phi_x d\boldsymbol{x} - \int_{J_j} \widehat{au_h}\phi(x^-_{i+\frac{1}{2}}, y)dy + \int_{J_j} \widehat{au_h}\phi(x^+_{i-\frac{1}{2}}, y)dy = -\int_{K_{i,j}} a_x u_h\phi d\boldsymbol{x}, \tag{2.7}$$

$$\int_{K_{i,j}} q_h^2\varphi d\boldsymbol{x} + \int_{K_{i,j}} au_h\varphi_y d\boldsymbol{x} - \int_{I_i} \widetilde{au_h}\varphi(x, y^-_{j+\frac{1}{2}})dx + \int_{I_i} \widetilde{au_h}\varphi(x, y^+_{j-\frac{1}{2}})dx = -\int_{K_{i,j}} a_y u_h\varphi d\boldsymbol{x}, \tag{2.8}$$

for all test functions ψ, ϕ, $\varphi \in V_h^k$. The hatted terms, $\widehat{aq_h^1}$ and $\widehat{au_h}$, and the tilde terms, $\widetilde{aq_h^2}$ and $\widetilde{au_h}$, in (2.6)-(2.8) are the cell boundary terms obtained from integration by parts, and they are the so-called numerical fluxes. These numerical fluxes are single-valued functions defined on the cell boundaries, and they are essential to ensure numerical stability and capture certain properties of the PDEs, such as energy conservation in wave equations.

If the function $a(\boldsymbol{x})$ is continuous, the numerical fluxes can be determined following the one-dimensional approach in [44]. For the hatted terms, we use the simple alternating fluxes,

$$\widehat{aq_h^1} = aq_h^{1,-}, \qquad \widehat{au_h} = au_h^+, \tag{2.9}$$

where all quantities are computed at the same points $(x_{i+1/2}, y)$ (i.e., the cell interface). We remark that the choice of the fluxes (2.9) is not unique. We can, for example, alternatively

choose the numerical fluxes to be

$$\widehat{aq_h^1} = aq_h^{1,+}, \qquad \widehat{au_h} = au_h^-. \tag{2.10}$$

Similarly, one can use the numerical fluxes

$$\widetilde{aq_h^2} = aq_h^{2,-}, \qquad \widetilde{au_h} = au_h^+, \tag{2.11}$$

or

$$\widetilde{aq_h^2} = aq_h^{2,+}, \qquad \widetilde{au_h} = au_h^-, \tag{2.12}$$

where all quantities are computed at the same points $(x, y_{j+\frac{1}{2}})$ (i.e., the cell interface).

However, if the function $a(\boldsymbol{x})$ is discontinuous, the above numerical fluxes are not well defined at the interface, since $a(\boldsymbol{x})$ takes different values from both sides of the interface. Here we assume that $a(\boldsymbol{x})$ is piecewise smooth and the discontinuities only occur in the direction aligned with our spatial discretization, namely, either vertical or horizontal (or both). Thus, we can align the jumps of $a(\boldsymbol{x})$ with cell interfaces. Then, one way to define the numerical fluxes is to take $a(\boldsymbol{x})$ from the same side as u_h or q_h^1 (or q_h^2), for example (2.9) becomes

$$\widehat{aq_h^1} = a^- q_h^{1,-}, \qquad \widehat{au_h} = a^+ u_h^+. \tag{2.13}$$

However, this is not sufficient to render the correct accuracy and energy preserving property. Theoretically, the natural interface condition (see [8]) for the two media is the continuity in u and the flux aq, that is, $u^- = u^+$ and $a^- q^- = a^+ q^+$. This continuity condition, however, is not consistent with the fluxes of the original LDG methods (2.7)-(2.8). Take Eq. (2.7) with the choice of numerical fluxes (2.13) as an example. Applying the integration by parts on the volume integral again, Eq. (2.7) becomes

$$\int_{K_{i,j}} q_h^1 \phi d\boldsymbol{x} - \int_{K_{i,j}} a(u_h)_x \phi d\boldsymbol{x} + \int_{J_j} \left(a^- u_h^- - a^+ u_h^+\right) \phi(x^+_{i-\frac{1}{2}}, y) dy = 0, \tag{2.14}$$

and this flux term $a^- u_h^- - a^+ u_h^+$ is not consistent with the continuity condition, as u, not au, is continuous across the interface.

To overcome this difficulty, we propose to update the discretization of Eqs. (2.7) and (2.8) by:

$$\int_{K_{i,j}} q_h^1 \phi d\boldsymbol{x} + \int_{K_{i,j}} u_h a \phi_x d\boldsymbol{x} - \int_{J_j} \widehat{u_h} a^- \phi(x^-_{i+\frac{1}{2}}, y) dy + \int_{J_j} \widehat{u_h} a^+ \phi(x^+_{i-\frac{1}{2}}, y) dy = -\int_{K_{i,j}} a_x u_h \phi d\boldsymbol{x}, \tag{2.15}$$

$$\int_{K_{i,j}} q_h^2 \varphi d\boldsymbol{x} + \int_{K_{i,j}} u_h a \varphi_y d\boldsymbol{x} - \int_{I_i} \widetilde{u_h} a^- \varphi(x, y^-_{j+\frac{1}{2}}) dx + \int_{I_i} \widetilde{u_h} a^+ \varphi(x, y^-_{j-\frac{1}{2}}) dx = -\int_{K_{i,j}} a_y u_h \varphi d\boldsymbol{x}, \tag{2.16}$$

for all test functions ψ, ϕ, $\varphi \in V_h^k$. Note that a is no longer included in the numerical flux and takes its value from inside the cell $K_{i,j}$, the same way as the test function φ, at the interface. We will show later that this choice of discretization will provide correct accuracy and energy conservation property. For the hatted terms, we still use the simple alternating fluxes,

$$\widehat{aq_h^1} = a^- q_h^{1,-}, \qquad \widehat{u_h} = u_h^+, \tag{2.17}$$

or

$$\widehat{aq_h^1} = a^+ q_h^{1,+}, \qquad \widehat{u_h} = u_h^-, \tag{2.18}$$

where all quantities are computed at the same points $(x_{i+\frac{1}{2}}, y)$ (i.e., the cell interface). Similarly, one can use the numerical fluxes

$$\widetilde{aq_h^2} = a^- q_h^{2,-}, \qquad \widetilde{u_h} = u_h^+, \tag{2.19}$$

or

$$\widetilde{aq_h^1} = a^+ q_h^{2,+}, \qquad \widetilde{u_h} = u_h^-, \tag{2.20}$$

where all quantities are computed at the same points $(x, y_{j+\frac{1}{2}})$ (i.e., the cell interface).

If the numerical fluxes (2.18) and (2.20) are used, and if we denote $K_{i,j}$ by K for simple presentation, the LDG methods can be equivalently reformulated as

$$((u_h)_{tt}, \psi)_K + (a\boldsymbol{q}_h, \nabla\psi)_K - (a^+ \boldsymbol{q}_h^+ \cdot \boldsymbol{\nu}, \psi)_{\partial K} = 0, \tag{2.21}$$

$$(\boldsymbol{q}_h, \boldsymbol{\phi})_K + (au_h, \nabla \cdot \boldsymbol{\phi})_K - (u_h^-, a\boldsymbol{\phi} \cdot \boldsymbol{\nu})_{\partial K} = -(u_h \nabla a, \boldsymbol{\phi})_K. \tag{2.22}$$

where $(\cdot)_K$ denotes the L^2 inner product, that is, $(\boldsymbol{f},\boldsymbol{g})_K = \int_K \boldsymbol{f}\cdot\boldsymbol{g}\ d\boldsymbol{x}$; the vector $\boldsymbol{\nu}$ is the outward normal vector of ∂K, and $\boldsymbol{\phi}$ is a vectored test function in the space $V_h^k \times V_h^k$. Equation (2.22) renders a formulation of $\boldsymbol{q}_h$ in terms of u_h in an element-by-element fashion, and therefore this could be substituted into Eq. (2.21). This is the spirit of the LDG method, and $\boldsymbol{q}_h$ is simply an auxiliary variable.

2.4 Energy conservation

As is well known, the important physical quantity, the energy $E = \int_\Omega u_t^2 + (a(\boldsymbol{x})u_x)^2 + (a(\boldsymbol{x})u_y)^2\ d\boldsymbol{x}$, is conserved, in the linear wave equation (2.1) with proper boundary conditions. This property is often taken into consideration in the design of numerical schemes because experiences show that schemes conserving the discrete analogs of energy appear to approximate the solution better, especially in the long time behavior. In this subsection, we will show that the proposed semi-discrete LDG method conserves energy.

Proposition 2.1. *The (continuous) energy*

$$E_h(t) = \int_\Omega \left((u_h)_t^2 + (q_h^1)^2 + (q_h^2)^2\right) dx \tag{2.23}$$

is conserved by the the semi-discrete LDG method (2.21)-(2.22) *for all time.*

Proof. By taking the time derivative of Eq. (2.22), and choosing the test function $\boldsymbol{\phi} = \boldsymbol{q}_h$, one obtains

$$((\boldsymbol{q}_h)_t, \boldsymbol{q}_h)_K + (a(u_h)_t, \nabla\cdot\boldsymbol{q}_h)_K - ((u_h^-)_t, a\boldsymbol{q}_h\cdot\boldsymbol{\nu})_{\partial K} = -((u_h)_t\nabla a, \boldsymbol{q}_h)_K. \tag{2.24}$$

In Eq. (2.21), we choose the test function to be $(u_h)_t$:

$$((u_h)_{tt}, (u_h)_t)_K + (a\boldsymbol{q}_h, \nabla(u_h)_t)_K - (a^+\boldsymbol{q}_h^+\cdot\boldsymbol{\nu}, (u_h)_t)_{\partial K} = 0. \tag{2.25}$$

Addition of Eq. (2.24) and Eq. (2.25) becomes

$$\begin{aligned}((u_h)_{tt}, (u_h)_t)_K + ((\boldsymbol{q}_h)_t, \boldsymbol{q}_h)_K + (a\boldsymbol{q}_h, \nabla(u_h)_t)_K + (a(u_h)_t, \nabla\cdot\boldsymbol{q}_h)_K \\ + (u_t\nabla a, \boldsymbol{q}_h)_K - ((u_h^-)_t, a\boldsymbol{q}_h\cdot\boldsymbol{\nu})_{\partial K} - (a^+\boldsymbol{q}_h^+\cdot\boldsymbol{\nu}, (u_h)_t)_{\partial K} = 0,\end{aligned}$$

and with integration by parts, we obtain

$$((u_h)_{tt},(u_h)_t)_K+((\boldsymbol{q}_h)_t,\boldsymbol{q}_h)_K+((u_h)_t,a\boldsymbol{q}_h\cdot\boldsymbol{\nu})_{\partial K}-((u_h^-)_t,a\boldsymbol{q}_h\cdot\boldsymbol{\nu})_{\partial K}-((u_h)_t,a^+\boldsymbol{q}_h^+\cdot\boldsymbol{\nu})_{\partial K}=0. \tag{2.26}$$

By summing up Eq. (2.26) over all cells and using the periodic or homogeneous Dirichlet boundary conditions, we have

$$\begin{aligned}0&=((u_h)_{tt},(u_h)_t)_\Omega+((\boldsymbol{q}_h)_t,\boldsymbol{q}_h)_\Omega+\sum_{K\in\mathcal{T}_h}\left(((u_h)_t,a\boldsymbol{q}_h\cdot\boldsymbol{\nu})_{\partial K}-((u_h^-)_t,a\boldsymbol{q}_h\cdot\boldsymbol{\nu})_{\partial K}-((u_h)_t,a^+\boldsymbol{q}_h^+\cdot\boldsymbol{\nu})_{\partial K}\right)\\&=((u_h)_{tt},(u_h)_t)_\Omega+((\boldsymbol{q}_h)_t,\boldsymbol{q}_h)_\Omega.\end{aligned}$$

Therefore the quantity E_h is invariant in time. □

3 Error estimate

In this section, we derive the optimal error estimates for the energy conserving LDG method (2.21)-(2.22) proposed in Section 2. The error estimate in the energy norm will be presented first, and then the analysis will be extended to the L^2 norm. We will also show that these error bounds are both linear in time.

3.1 Projections and inequalities

First, we introduce the projections and other notations that will be used throughout this paper. We use P to denote a weighted L^2 projection of a function $\omega(x)$ with $k+1$ continuous derivatives into space V_h^k, that is:

$$(P\omega,a\phi)_K=(\omega,a\phi)_K,$$

for any $\phi\in Q^k$ on K.

In addition, a one-dimensional projection P_x^- for a real-valued function ω, which projects ω into the one-dimensional piecewise polynomial space of degree k while taking the values of ω at the cell interface, is defined as follows

$$(P_x^-\omega,a\phi)_{I_i}=(\omega,a\phi)_{I_i},\quad\forall\phi\in P^{k-1}(I_i)\quad\text{and}\quad(P_x^-\omega)^-(x_{i+\frac{1}{2}})=\omega^-(x_{i+\frac{1}{2}}), \tag{3.1}$$

where $P^{k-1}(I_i)$ is the space of polynomials on the interval I_i of degree up to $k-1$. Similarly, the one-dimensional projection $P_x^+\omega$ is defined as the projection of ω such that

$$(P_x^+\omega, a\phi)_{I_i} = (\omega, a\phi)_{I_i}, \quad \forall \phi \in P^{k-1}(I_i) \quad \text{and} \quad (P_x^+\omega)^+(x_{i-\frac{1}{2}}) = \omega^+(x_{i-\frac{1}{2}}),$$

and the one-dimensional projection on the y-direction $P_y^\pm$ are defined in the same way. Since the Cartesian meshes are used in this paper, we can extend the definition of the above $P_x^\pm$ to two dimension: on a two-dimensional rectangular element $K_{i,j} = I_i \times J_j$, the projection P^- for scalar functions are defined as

$$P^- = P_x^- \otimes P_y^-. \tag{3.2}$$

This projection P^- on the Cartesian meshes has been shown in [23, Lemma 3.7] to have the following superconvergence property: for $\eta \in H^{k+2}(\Omega)$, $\boldsymbol{\rho} \in \Sigma_h^k$,

$$|(\eta - P^-\eta, a\nabla\cdot\boldsymbol{\rho})_{\mathcal{T}_h} - (\eta - \widehat{P^-\eta}, a\boldsymbol{\rho}\cdot\nu)_{\mathcal{E}_h}| \le Ch^{k+1}\|\eta\|_{H^{k+2}(\Omega)}\|\boldsymbol{\rho}\|_\Omega, \tag{3.3}$$

where the "hat" term denotes the numerical flux.

Another projection $\boldsymbol{\Pi}^+$, for vector-valued functions $\boldsymbol{\rho} = (\rho_1, \rho_2)$, is defined as

$$\boldsymbol{\Pi}^+\boldsymbol{\rho} = (P_x^+ \otimes P_y\rho_1,\ P_x \otimes P_y^+\rho_2), \tag{3.4}$$

where P_x and P_y are the one-dimensional L^2 projections in the x- and y-directions, respectively. One can easily observe that, for any $\boldsymbol{\rho} \in [H^1(\Omega)]^2$, the restriction of $\boldsymbol{\Pi}^+\boldsymbol{\rho}$ to $I \times J$ $(= K_{i,j})$ are elements of $[Q^k(I \times J)]^2$ that satisfy

$$(\boldsymbol{\Pi}^+\boldsymbol{\rho} - \boldsymbol{\rho}, a\nabla w)_{I\times J} = 0, \tag{3.5}$$

for any $w \in Q^k(I \times J)$, and

$$\left((\boldsymbol{\Pi}^+\boldsymbol{\rho}(x_{i-\frac{1}{2}}, \cdot) - \boldsymbol{\rho}(x_{i-\frac{1}{2}}, \cdot))\cdot\boldsymbol{\nu}, aw(x^+_{i-\frac{1}{2}}, \cdot)\right)_J = 0, \quad \forall w \in Q^k(I \times J), \tag{3.6}$$

$$\left((\boldsymbol{\Pi}^+\boldsymbol{\rho}(\cdot, y_{j-\frac{1}{2}}) - \boldsymbol{\rho}(\cdot, y_{j-\frac{1}{2}}))\cdot\boldsymbol{\nu}, aw(\cdot, y^+_{j-\frac{1}{2}})\right)_I = 0, \quad \forall w \in Q^k(I \times J), \tag{3.7}$$

where $\boldsymbol{\nu}$ is the outward normal vector of the boundary of K_{ij}. These projections defined above have the following approximation property (see [23, 45]): for any $\eta \in H^{k+1}(\Omega)$ and $\boldsymbol{\rho} \in [H^{k+1}(\Omega)]^2$,

$$\|P^{\pm}\eta - \eta\|_{\Omega} \leq Ch^{k+1}\|\eta\|_{H^{k+1}(\Omega)}, \qquad \|\boldsymbol{\Pi}^{\pm}\boldsymbol{\rho} - \boldsymbol{\rho}\|_{\Omega} \leq Ch^{k+1}\|\boldsymbol{\rho}\|_{H^{k+1}(\Omega)}, \tag{3.8}$$

where C is independent of the mesh size h.

Finally, we denote the errors by

$$\begin{aligned} &e_u = u - u_h = \eta_u + \zeta_u, \qquad \eta_u = u - P^{-}u, \qquad \zeta_u = P^{-}u - u_h, \\ &e_{\boldsymbol{q}} = \boldsymbol{q} - \boldsymbol{q}_h = \eta_{\boldsymbol{q}} + \zeta_{\boldsymbol{q}}, \qquad \eta_{\boldsymbol{q}} = \boldsymbol{q} - \boldsymbol{\Pi}^{+}\boldsymbol{q}, \qquad \zeta_{\boldsymbol{q}} = \boldsymbol{\Pi}^{+}\boldsymbol{q} - \boldsymbol{q}_h, \end{aligned} \tag{3.9}$$

which, from left to right, respectively represent the errors between the exact solution and the numerical solution, the projection errors, and the errors between the numerical solution and the particular projection of the exact solution. Note that the signs of the projection $P_h^{\pm}$ and $\boldsymbol{\Pi}^{\pm}$ of u and $\boldsymbol{q}$ in (3.9) are consistent with the choice of the numerical fluxes in (2.17). So if the other set of numerical fluxes are chosen, the signs of $P_h^{\pm}$ and $\boldsymbol{\Pi}^{\pm}$ in (3.9) should be changed accordingly.

3.2 Error estimate in the energy norm

The optimal error estimates of the proposed LDG method rely upon carefully chosen projections of the initial conditions. Note that we have two initial conditions in (2.2), one for u and the other for u_t. We take the initial condition $u_h(\boldsymbol{x}, 0)$ as $P_h^{-}u(\boldsymbol{x}, 0) = P_h^{-}u_0(\boldsymbol{x})$, which is consistent with the choice of the numerical fluxes (2.17). The other initial condition $(u_h)_t(\boldsymbol{x}, 0)$ is given by the standard L^2 projection. Thus, we have the following lemma.

Lemma 3.1. *Suppose the initial conditions of the LDG scheme* (2.6)-(2.7) *are given by*

$$u_h(\boldsymbol{x}, 0) = P_h^{-}u(\boldsymbol{x}, 0), \qquad (u_h)_t(\boldsymbol{x}, 0) = P_h u_t(\boldsymbol{x}, 0), \tag{3.10}$$

there holds the following error estimates

$$\|\zeta_u(0)\| = 0, \qquad \|\zeta_{\boldsymbol{q}}(0)\| \leq Ch^{k+1}, \qquad \|(\zeta_u)_t(0)\| \leq Ch^{k+1}, \tag{3.11}$$

and

$$((e_u)_t(0), v)_\Omega = 0, \quad \text{for any } v \in Q^k. \tag{3.12}$$

The proof of this Lemma is similar as that in [44], and is therefore omitted here.

Remark 3.1. *We would like to emphasize that this special choice of initial condition is critical in the optimal convergence rate of the proposed LDG method. The optimal error estimate shown below is based on these initial conditions, and this is confirmed by our numerical experiments. As shown in Section 5, if the standard L^2 projections are used for both u and u_t, the convergence rate becomes oscillating and does not converge to the desired $(k+1)$-th order accuracy. Although previous studies on LDG methods showed that the different choices of initial condition have little impact on the convergence/superconvergence results [11, 37, 32], different initial conditions do make a difference for our method. We believe it is related to the fact that the current energy conserving method has no numerical dissipation, and therefore it is more sensitive to the error in the initial conditions. So it is critical to choose an appropriate initial condition which results in the "optimal" energy-conserving method.*

Based on the initial conditions (3.10), we have the following error estimate in the energy norm.

Proposition 3.1. *Let u and $\boldsymbol{q}$ be the exact solutions of the wave equation* (2.5)*, and u_h, $\boldsymbol{q}_h$ be the numerical solutions of the semi-discrete LDG method* (2.21)-(2.22) *with the initial conditions* (3.10)*, there holds the following error estimates:*

$$\|(e_u)_t\| \le Ch^{k+1}(t+1), \qquad \|e_{\boldsymbol{q}}\| \le Ch^{k+1}(t+1), \tag{3.13}$$

where the constant C depends on $\max_{K\in\mathcal{T}_h}\{\|\nabla a(x)\|_\infty | x \in K\}$, $\|u\|_{H^{k+3}}$ and $\|u_t\|_{H^{k+2}}$.

Proof. The error equations of the proposed LDG method are

$$((e_u)_{tt}, \psi)_K + (ae_{\boldsymbol{q}}, \nabla\psi)_K - (a^+ e^+_{\boldsymbol{q}} \cdot \boldsymbol{\nu}, \psi)_{\partial K} = 0, \tag{3.14}$$

$$(e_{\boldsymbol{q}}, \boldsymbol{\phi})_K + (ae_u, \nabla\cdot\boldsymbol{\phi})_K - (e^-_u, a\boldsymbol{\phi}\cdot\boldsymbol{\nu})_{\partial K} = -(e_u\nabla a, \boldsymbol{\phi})_K, \tag{3.15}$$

for all test functions $\psi \in V_h^k$ and $\boldsymbol{\phi} \in \Sigma_h^k$, which can be derived by subtracting (2.21)-(2.22) from the weak formulation satisfied by the exact solutions u and q.

Using the properties of the projections P^- and $\boldsymbol{\Pi}^+$, the error equations become

$$((\zeta_u)_{tt}, \psi)_K + ((\eta_u)_{tt}, \psi)_K + (a\zeta_{\boldsymbol{q}}, \nabla\psi)_K - (a^+\zeta_{\boldsymbol{q}}^+ \cdot \boldsymbol{\nu}, \psi)_{\partial K} = 0, \tag{3.16}$$

$$\begin{aligned}&(\zeta_{\boldsymbol{q}}, \boldsymbol{\phi})_K + (\eta_{\boldsymbol{q}}, \boldsymbol{\phi})_K + (a\zeta_u, \nabla\cdot\boldsymbol{\phi})_K - (\zeta_u^-, a\boldsymbol{\phi}\cdot\boldsymbol{\nu})_{\partial K} + (a\eta_u, \nabla\cdot\boldsymbol{\phi})_K - (\eta_u^-, a\boldsymbol{\phi}\cdot\boldsymbol{\nu})_{\partial K}\\ &\quad = -(\zeta_u\nabla a, \boldsymbol{\phi})_K - (\eta_u\nabla a, \boldsymbol{\phi})_K,\end{aligned} \tag{3.17}$$

Along the same line in the proof of Proposition 2.1, we first take the time derivative of Eq. (3.17), choose the test functions to be $\boldsymbol{\phi} = \zeta_{\boldsymbol{q}}$, $\psi = (\zeta_u)_t$, and then sum up the resulting two equations to get

$$\begin{aligned}&((\zeta_u)_{tt}, (\zeta_u)_t)_K + ((\eta_u)_{tt}, (\zeta_u)_t)_K + ((\zeta_{\boldsymbol{q}})_t, \zeta_{\boldsymbol{q}})_K + ((\eta_{\boldsymbol{q}})_t, \zeta_{\boldsymbol{q}})_K =\\ &\quad -(a\zeta_{\boldsymbol{q}}, \nabla(\zeta_u)_t)_K + (a^+\zeta_{\boldsymbol{q}}^+\cdot\boldsymbol{\nu}, (\zeta_u)_t)_{\partial K} - (a(\zeta_u)_t, \nabla\cdot\zeta_{\boldsymbol{q}})_K + ((\zeta_u)_t^-, a\zeta_{\boldsymbol{q}}\cdot\boldsymbol{\nu})_{\partial K}\\ &\quad -(a(\eta_u)_t, \nabla\cdot\zeta_{\boldsymbol{q}})_K + ((\eta_u)_t^-, a\zeta_{\boldsymbol{q}}\cdot\boldsymbol{\nu})_{\partial K} - ((\zeta_u)_t\nabla a, \zeta_{\boldsymbol{q}})_K - ((\eta_u)_t\nabla a, \zeta_{\boldsymbol{q}})_K.\end{aligned}$$

If the Dirichlet boundary conditions are imposed, the flux terms of the boundary cells $\mathcal{E}_h^B$ in the above equations will vanish, and therefore for simplicity, we only keep the notation for the internal cells.

Summing up the above equation over all cells and using integration by parts yields

$$\begin{aligned}&((\zeta_u)_{tt}, (\zeta_u)_t)_{\mathcal{T}_h} + ((\eta_u)_{tt}, (\zeta_u)_t)_{\mathcal{T}_h} + ((\zeta_{\boldsymbol{q}})_t, \zeta_{\boldsymbol{q}})_{\mathcal{T}_h} + ((\eta_{\boldsymbol{q}})_t, \zeta_{\boldsymbol{q}})_{\mathcal{T}_h} =\\ &\quad -(a(\eta_u)_t, \nabla\cdot\zeta_{\boldsymbol{q}})_{\mathcal{T}_h} + ((\eta_u)_t^-, a\zeta_{\boldsymbol{q}}\cdot\boldsymbol{\nu})_{\mathcal{E}_h} - ((\eta_u)_t\nabla a, \zeta_{\boldsymbol{q}})_{\mathcal{T}_h}\end{aligned}$$

if periodic or Dirichlet boundary conditions are employed.

By the properties of the projections (3.3) and (3.8), one has

$$\begin{aligned}&\frac{1}{2}\frac{d}{dt}\left(\|(\zeta_u)_t\|^2 + \|\zeta_{\boldsymbol{q}}\|^2\right) = \frac{1}{2}\frac{d}{dt}\int_I \left((\zeta_u)_t^2 + \zeta_{\boldsymbol{q}}^2\right) dx\\ &\le |((\eta_u)_{tt}, (\zeta_u)_t)_{\mathcal{T}_h} + ((\eta_{\boldsymbol{q}})_t, \zeta_{\boldsymbol{q}})_{\mathcal{T}_h}| + Ch^{k+1}\|u_t\|_{H^{k+2}(\Omega)}\|\zeta_{\boldsymbol{q}}\| + |\nabla a|_\infty\|(\eta_u)_t\|\|\zeta_{\boldsymbol{q}}\|\\ &\le Ch^{k+1}\left(\|(\zeta_u)_t\| + \|\zeta_{\boldsymbol{q}}\|\right) \le Ch^{k+1}\left(\|(\zeta_u)_t\|^2 + \|\zeta_{\boldsymbol{q}}\|^2\right)^{\frac{1}{2}},\end{aligned}$$

which leads to

$$\frac{d}{dt}\left(\|(\zeta_u)_t\|^2+\|\zeta_{\boldsymbol{q}}\|^2\right)^{\frac{1}{2}}\leq Ch^{k+1}.$$

Combining this inequality with the property of the initial condition (3.11), we conclude that

$$\left(\|(\zeta_u)_t\|^2+\|\zeta_{\boldsymbol{q}}\|^2\right)^{\frac{1}{2}}\leq C(t+1)h^{k+1},$$

in which the constant C only depends on $\max_{K\in\mathcal{T}_h}\{\|\nabla a(x)\|_\infty|x\in K\}$, $\|u\|_{H^{k+3}}$ and $\|u_t\|_{H^{k+2}}$. Together with the optimal projection error (3.8), the error estimate (3.13) follows. □

3.3 Error estimate in the L^2 norm

In this section, we prove the optimal error estimate in the L^2 norm.

Proposition 3.2. *Let u and $\boldsymbol{q}$ be the exact solutions of the wave equation* (2.5)*, and u_h, $\boldsymbol{q}_h$ be the numerical solutions of the semi-discrete LDG method* (2.21)-(2.22) *with the initial conditions* (3.10)*, there holds the following error estimate:*

$$\max_{t\in[0,T]}\|e_u(t)\|\leq Ch^{k+1}(T+1), \tag{3.18}$$

where the constant C only depends on the solution u and a.

Proof. First, the term $(e_u)_{tt}$ is split as the summation of $(\zeta_u)_{tt}$ and $(\eta_u)_{tt}$ in Eq. (3.16), and by using product rule in time derivative, one obtains

$$-((\zeta_u)_t,\psi_t)_K+(a\zeta_{\boldsymbol{q}},\nabla\psi)_K-(a^+\zeta_{\boldsymbol{q}}^+\cdot\boldsymbol{\nu},\psi)_{\partial K}=-((\eta_u)_{tt},\psi)_K-\frac{d}{dt}((\zeta_u)_t,\psi)_K. \tag{3.19}$$

For any fixed time $\tau\leq T$, we denote the time integral of the error by

$$\begin{aligned}
E_u(t)&=\int_t^\tau e_u(s)ds,\quad E_u^\eta(t)=\int_t^\tau\eta_u(s)ds,\quad E_u^\zeta(t)=\int_t^\tau\zeta_u(s)ds,\\
E_{\boldsymbol{q}}(t)&=\int_t^\tau e_{\boldsymbol{q}}(s)ds,\quad E_{\boldsymbol{q}}^\eta(t)=\int_t^\tau\eta_{\boldsymbol{q}}(s)ds,\quad E_{\boldsymbol{q}}^\zeta(t)=\int_t^\tau\zeta_{\boldsymbol{q}}(s)ds.
\end{aligned}$$

Integrating Eq. (3.15) in time, from t to τ yields

$$(E_{\boldsymbol{q}},\boldsymbol{\phi})_K+(aE_u,\nabla\cdot\boldsymbol{\phi})_K-(E_u^-,a\boldsymbol{\phi}\cdot\boldsymbol{\nu})_{\partial K}=-(E_u\nabla a,\boldsymbol{\phi})_K. \tag{3.20}$$

If we choose the test functions to be $\psi = E_u^\zeta(t)$ and $\boldsymbol{\phi} = \zeta_{\boldsymbol{q}}(t)$ in (3.19)-(3.20), and use the fact that $\psi_t = -\zeta_u(t)$, we have

$$((\zeta_u)_t, \zeta_u)_K + (a\zeta_{\boldsymbol{q}}, \nabla E_u^\zeta)_K - (a^+\zeta_{\boldsymbol{q}}^+ \cdot \boldsymbol{\nu}, E_u^\zeta)_{\partial K} = -((\eta_u)_{tt}, E_u^\zeta)_K - \frac{d}{dt}((\zeta_u)_t, E_u^\zeta)_K, \quad (3.21)$$

$$\begin{aligned}&(E_{\boldsymbol{q}}^\zeta, \zeta_{\boldsymbol{q}})_K + (aE_u^\zeta, \nabla \cdot \zeta_{\boldsymbol{q}})_K - ((E_u^\zeta)^-, a\zeta_{\boldsymbol{q}} \cdot \boldsymbol{\nu})_{\partial K} + (E_u^\zeta \nabla a, \zeta_{\boldsymbol{q}})_K \\ &\quad = -(E_{\boldsymbol{q}}^\eta, \zeta_{\boldsymbol{q}})_K - (aE_u^\eta, \nabla \cdot \zeta_{\boldsymbol{q}})_K + ((E_u^\eta)^-, a\zeta_{\boldsymbol{q}} \cdot \boldsymbol{\nu})_{\partial K} - (E_u^\eta \nabla a, \zeta_{\boldsymbol{q}})_K. \quad (3.22)\end{aligned}$$

If the Dirichlet boundary conditions are used, the flux terms of the boundary cells $\mathcal{E}_h^B$ in the above equations will vanish, and therefore for simplicity, we only keep the notation for the internal cells.

Adding up Eqs. (3.21) and (3.22) and summing over all cells, and using the periodic or Dirichlet boundary conditions, one obtains

$$\begin{aligned}\frac{1}{2}\frac{d}{dt}\left(\|\zeta_u\|^2 - \|E_{\boldsymbol{q}}^\zeta\|^2\right) &= -((\eta_u)_{tt}, E_u^\zeta)_{\mathcal{T}_h} - \frac{d}{dt}((\zeta_u)_t, E_u^\zeta)_{\mathcal{T}_h} - (E_{\boldsymbol{q}}^\eta, \zeta_{\boldsymbol{q}})_{\mathcal{T}_h} \\ &\quad -(aE_u^\eta, \nabla \cdot \zeta_{\boldsymbol{q}})_{\mathcal{T}_h} + ((E_u^\eta)^-, a\zeta_{\boldsymbol{q}} \cdot \boldsymbol{\nu})_{\mathcal{E}_h} - (E_u^\eta \nabla a, \zeta_{\boldsymbol{q}})_{\mathcal{T}_h}.\end{aligned}$$

Integrating the above equation from 0 to τ, we get

$$\begin{aligned}&\frac{1}{2}\|\zeta_u(\tau)\|^2 - \frac{1}{2}\|\zeta_u(0)\|^2 + \frac{1}{2}\|E_{\boldsymbol{q}}^\zeta(0)\|^2 \\ &\qquad = -\int_0^\tau ((\eta_u)_t, \zeta_u)_{\mathcal{T}_h} dt + ((e_u)_t(0), E_u^\zeta(0))_{\mathcal{T}_h} - \int_0^\tau (E_{\boldsymbol{q}}^\eta, \zeta_{\boldsymbol{q}})_{\mathcal{T}_h} dt \\ &\qquad + \int_0^\tau \left(-(aE_u^\eta, \nabla \cdot \zeta_{\boldsymbol{q}})_{\mathcal{T}_h} + ((E_u^\eta)^-, a\zeta_{\boldsymbol{q}} \cdot \boldsymbol{\nu})_{\mathcal{E}_h} - (E_u^\eta \nabla a, \zeta_{\boldsymbol{q}})_{\mathcal{T}_h}\right) dt, \quad (3.23)\end{aligned}$$

in which we use the fact $E_{\boldsymbol{q}}^\zeta(\tau) = E_u^\zeta(\tau) = 0$. By the property of the projection (3.8), we have $\|(E_u^\eta)_t\| = Ch^{k+1}$. Note that

$$E_{\boldsymbol{q}}^\eta(t) = \int_t^\tau \eta_{\boldsymbol{q}}(s) ds = \int_t^\tau \left(\boldsymbol{q}(s) - P^-\boldsymbol{q}(s)\right) ds = \int_t^\tau \boldsymbol{q}(s) ds - P^-\left(\int_t^\tau \boldsymbol{q}(s) ds\right),$$

and therefore we can conclude that $\|E_{\boldsymbol{q}}^\eta\| = Ch^{k+1}$. Due to the property of projection P^- (3.3), one has

$$\begin{aligned}&-(aE_u^\eta, \nabla \cdot \zeta_{\boldsymbol{q}})_{\mathcal{T}_h} + ((E_u^\eta)^-, a\zeta_{\boldsymbol{q}} \cdot \boldsymbol{\nu})_{\mathcal{E}_h} - (E_u^\eta \nabla a, \zeta_{\boldsymbol{q}})_{\mathcal{T}_h} \\ &\quad \le Ch^{k+1}\|\zeta_{\boldsymbol{q}}\|_\Omega + |\nabla a|_\infty \|E_u^\eta\|_\Omega \|\zeta_{\boldsymbol{q}}\|_\Omega \le Ch^{2k+2}(T+1),\end{aligned}$$

where the last inequality comes from the error estimate (3.13) of $\boldsymbol{q}$. Combining with the property of the L^2 projection (3.12), we have

$$\begin{aligned}
&\frac{1}{2}\|\zeta_u(\tau)\|^2 - \frac{1}{2}\|\zeta_u(0)\|^2 + \frac{1}{2}\|E_{\boldsymbol{q}}^{\zeta}(0)\|^2 \\
&\qquad \le \left|\int_0^\tau ((\eta_u)_t, \zeta_u)_{\mathcal{T}_h} dt\right| + \left|\int_0^\tau (E_{\boldsymbol{q}}^{\eta}, \zeta_{\boldsymbol{q}})_{\mathcal{T}_h} dt\right| + Ch^{2k+2}(T+1)\tau \\
&\qquad \le \int_0^\tau \|(\eta_u)_t\|\|\zeta_u\| dt + \int_0^\tau \|E_{\boldsymbol{q}}^{\eta}\|\|\zeta_{\boldsymbol{q}}\| dt + Ch^{2k+2}(T+1)\tau \\
&\qquad \le \tau \max_{t\in[0,\tau]} \|(\eta_u)_t\| \max_{t\in[0,\tau]} \|\zeta_u\| + \tau \max_{t\in[0,\tau]} \|E_{\boldsymbol{q}}^{\eta}\| \max_{t\in[0,\tau]} \|\zeta_{\boldsymbol{q}}\| + Ch^{2k+2}(T+1)\tau \\
&\qquad \le T\left(\max_{t\in[0,T]} \|(\eta_u)_t\| \max_{t\in[0,T]} \|\zeta_u\| + \max_{t\in[0,T]} \|E_{\boldsymbol{q}}^{\eta}\| \max_{t\in[0,T]} \|\zeta_{\boldsymbol{q}}\| + Ch^{2k+2}(T+1)\right) \\
&\qquad \le CT\left(h^{k+1} \max_{t\in[0,T]} \|\zeta_u\| + (T+1)h^{2k+2}\right) \\
&\qquad \le C(T^2+1)h^{2k+2} + \frac{1}{4}\max_{t\in[0,T]} \|\zeta_u\|^2.
\end{aligned}$$

Since this is true for any $\tau < T$, we have

$$\frac{1}{2}\|\zeta_u(\tau)\|^2 - \frac{1}{2}\|\zeta_u(0)\|^2 + \frac{1}{2}\|E_{\boldsymbol{q}}^{\zeta}(0)\|^2 \;\le\; C(T^2+1)h^{2k+2} + \frac{1}{4}\max_{t\in[0,T]} \|\zeta_u\|^2.$$

Hence,

$$\frac{1}{4}\max_{t\in[0,T]} \|\zeta_u\|^2 + \frac{1}{2}\|E_{\boldsymbol{q}}^{\zeta}(0)\|^2 \;\le\; C(T^2+1)h^{2k+2} + \frac{1}{2}\|\zeta_u(0)\|^2 = C(T^2+1)h^{2k+2},$$

from which we can conclude

$$\max_{t\in[0,T]} \|e_u(t)\| \le Ch^{k+1}(T+1).$$

where the constant C only depends on the solution u and a. □

Remark 3.2. *The proposed semi-discrete LDG method has the advantage of energy conserving and optimal convergence rate. The proof of optimal error estimate is carried out with the Q^k polynomial space. Numerically, if one uses P^k space ($P^k = \{x^{k_1}y^{k_2} | k_1 + k_2 \le k\}$), the same results can be observed, as shown in Section 5. However it seems to be difficult to prove this fact, as the special projection introduced in the subsection 3.1 does not exist in the P^k space.*

4 Time discretization

In this section, we develop fully discrete method that maintains the energy conservation property of the semi-discrete methods. To achieve this, it is essential to employ time stepping methods that conserve the discrete energy. In the following, we introduce a second-order time stepping (leap frog), and a high order symplectic time integrator.

In general, one obtains the semi-discrete scheme (2.21)-(2.22) after the spatial discretization by the LDG method. Note that we can solve $\boldsymbol{q}_h$ in terms of u_h in (2.22) in an element-by-element fashion. This local solvability gives the name to the LDG method, and we refer to [18] for details. Eliminating the auxiliary variable $\boldsymbol{q}_h$ leads to the linear second-order ordinary differential system:

$$M\ddot{\boldsymbol{u}}_h(t) = A\boldsymbol{u}_h(t), \tag{4.1}$$

where $\boldsymbol{u}_h(t)$ denotes the solution vector at time t and M denotes the mass matrix.

4.1 Second order time stepping

Newmark method is a family of single-step integration methods, proposed by Newmark [39] in 1959, for the solution of structural dynamics problems. It has been applied to dynamics analysis of many practical engineering problems during the last forty years. In [34], Newmark method is shown to belong to the category of variational algorithms, which are well known to be symplectic and momentum preserving and to often have excellent global energy behaviour. A special case in the Newmark family is the standard leap-frog method, which is well-known to be energy conserving.

Let $0 \le t_0 < t_1 < \cdots < t_N = T$ be a partition of the interval $[0, T]$ with time step $\Delta t_n = t_{n+1} - t_n$. Here uniform time step Δt is used. The fully discrete approximations u_h^n to $u(\cdot, t_n)$ are constructed as follows: for $n = 1, \ldots, N-1$, $u_h^{n+1} \in V_h^k$ is given by

$$M\frac{\boldsymbol{u}_h^{n+1} - 2\boldsymbol{u}_h^n + \boldsymbol{u}_h^{n-1}}{\Delta t^2} = A\boldsymbol{u}_h^n, \tag{4.2}$$

based on the system (4.1), and more precisely,

$$\left(\frac{u_h^{n+1}-2u_h^n+u_h^{n-1}}{\Delta t^2},\psi\right)_K+(a\boldsymbol{q}_h^n,\nabla\psi)_K-(a^+(\boldsymbol{q}^n)_h^+\cdot\boldsymbol{\nu},\psi)_{\partial K}=0, \tag{4.3}$$

$$(\boldsymbol{q}_h^n,\boldsymbol{\phi})_K+(au_h^n,\nabla\cdot\boldsymbol{\phi})_K-((u_h^n)^-,a\boldsymbol{\phi}\cdot\boldsymbol{\nu})_{\partial K}=-(u_h^n\nabla a,\boldsymbol{\phi})_K, \tag{4.4}$$

for all test functions $\psi\in V_h^k$ and $\boldsymbol{\phi}\in\Sigma_h^k$. The initial u_h^0 and u_h^1 can be obtained through projection and Taylor expansion, and this is shown in Eqs. (5.2) and (5.3) in Section 5.1.1. The stability condition is the standard Leap-Frog condition, where the CFL number should be less than 1.

In Proposition 2.1, we have shown the semi-discrete LDG method conserves the continuous energy $E_h(t)$. Along the same line of analysis, we can prove that the discrete energy, as defined in the following proposition, is conserved in the fully discrete method.

Proposition 4.1. *The solution to the fully discrete leap-frog LDG method* (4.3)-(4.4)*, conserves the (discrete) energy*

$$E_h^{n+1}=\left\|\frac{u_h^{n+1}-u_h^n}{\Delta t}\right\|^2+\left\|\frac{\boldsymbol{q}_h^{n+1}+\boldsymbol{q}_h^n}{2}\right\|^2-\frac{\Delta t^2}{4}\left\|\frac{\boldsymbol{q}_h^{n+1}-\boldsymbol{q}_h^n}{\Delta t}\right\|^2 \tag{4.5}$$

for all n.

Proof. We choose the test function in (4.3) to be $\psi=(u_h^{n+1}-u_h^n)/(2\Delta t)+(u_h^n-u_h^{n-1})/(2\Delta t)=(u_h^{n+1}-u_h^{n-1})/(2\Delta t)$, and obtain

$$\begin{aligned}\left(\frac{u_h^{n+1}-2u_h^n+u_h^{n-1}}{\Delta t^2},\frac{u_h^{n+1}-u_h^{n-1}}{2\Delta t}\right)_K+\left(a\boldsymbol{q}_h^n,\nabla\left(\frac{u_h^{n+1}-u_h^{n-1}}{2\Delta t}\right)\right)_K \\ -\left(a^+(\boldsymbol{q}^n)_h^+\cdot\boldsymbol{\nu},\frac{u_h^{n+1}-u_h^{n-1}}{2\Delta t}\right)_{\partial K} &= 0.\end{aligned} \tag{4.6}$$

Consider Eq. (4.4) at time levels t^{n-1} and t^{n+1}, and let the test function $\boldsymbol{\phi}$ be $q_h^n/(2\Delta t)$. Subtracting these two equations yields

$$\begin{aligned}\left(\frac{\boldsymbol{q}_h^{n+1}-\boldsymbol{q}_h^{n-1}}{2\Delta t},\boldsymbol{q}_h^n\right)_K+\left(a\frac{u_h^{n+1}-u_h^{n-1}}{2\Delta t},\nabla\cdot\boldsymbol{q}_h^n\right)_K \\ -\left(\frac{(u_h^{n+1})^--(u_h^{n-1})^-}{2\Delta t},a\boldsymbol{q}_h^n\cdot\boldsymbol{\nu}\right)_{\partial K}=-\left(\frac{u_h^{n+1}-u_h^{n-1}}{2\Delta t}\nabla a,\boldsymbol{q}_h^n\right)_K.\end{aligned} \tag{4.7}$$

Adding Eqs. (4.6) to (4.7) and summing over all cells gives

$$
\begin{aligned}
&\left(\frac{u_h^{n+1}-2u_h^n+u_h^{n-1}}{\Delta t^2},\frac{u_h^{n+1}-u_h^{n-1}}{2\Delta t}\right)_{\mathcal{T}_h}+\left(\frac{\boldsymbol{q}_h^{n+1}-\boldsymbol{q}_h^{n-1}}{2\Delta t},\boldsymbol{q}_h^n\right)_{\mathcal{T}_h}\\
&=\left(\frac{u_h^{n+1}-2u_h^n+u_h^{n-1}}{\Delta t^2},\frac{u_h^{n+1}-u_h^{n-1}}{2\Delta t}\right)_{\mathcal{T}_h}+\left(\frac{\boldsymbol{q}_h^{n+1}+2\boldsymbol{q}_h^n+\boldsymbol{q}_h^{n-1}}{4},\frac{\boldsymbol{q}_h^{n+1}-\boldsymbol{q}_h^{n-1}}{2\Delta t}\right)_{\mathcal{T}_h}\\
&\qquad-\left(\frac{\boldsymbol{q}_h^{n+1}-2\boldsymbol{q}_h^n+\boldsymbol{q}_h^{n-1}}{4},\frac{\boldsymbol{q}_h^{n+1}-\boldsymbol{q}_h^{n-1}}{2\Delta t}\right)_{\mathcal{T}_h}\\
&=\frac{1}{2\Delta t}\left(\left\|\frac{u_h^{n+1}-u_h^n}{\Delta t}\right\|^2+\left\|\frac{\boldsymbol{q}_h^{n+1}+\boldsymbol{q}_h^n}{2}\right\|^2-\frac{\Delta t^2}{4}\left\|\frac{\boldsymbol{q}_h^{n+1}-\boldsymbol{q}_h^n}{\Delta t}\right\|^2\right.\\
&\qquad\left.-\left\|\frac{u_h^{n}-u_h^{n-1}}{\Delta t}\right\|^2-\left\|\frac{\boldsymbol{q}_h^{n}+\boldsymbol{q}_h^{n-1}}{2}\right\|^2+\frac{\Delta t^2}{4}\left\|\frac{\boldsymbol{q}_h^{n}-\boldsymbol{q}_h^{n-1}}{\Delta t}\right\|^2\right)\\
&=0.
\end{aligned}
$$

Therefore, by the definition of E_h^n in (4.5), we have $E_h^{n+1}=E_h^n$ for all n, which completes the proof. □

Remark 4.1. *The discrete energy E_h^n can be rewritten as:*

$$E_h^{n+1}=\int_\Omega\left(\frac{u_h^{n+1}-u_h^n}{\Delta t}\right)^2dx+\int_\Omega\boldsymbol{q}_h^{n+1}\boldsymbol{q}_h^n dx, \tag{4.8}$$

which is a consistent approximation of the continuous energy (2.23).

4.2 High order time stepping

The spatial discretization of the proposed method is by the local discontinuous Galerkin method, which can be high order accurate depending on the polynomial degree k utilized in the space V_h^k. Therefore, we would like to present high order time stepping which also conserves the energy exactly. Such numerical methods have been designed from the modified equation approach [42, 22, 43]. Following the same technique, we will present an energy-conserving fourth-order time discretization below. This idea can be extended to derive higher order methods.

For a smooth function u, simple calculus leads to

$$u(t+\Delta t)-2u(t)+u(t-\Delta t)=\Delta t^2\int_{-1}^{1}(1-|\theta|)u''(t+\theta\Delta t)d\theta. \tag{4.9}$$

Therefore, the leap-frog method is obtained by simply approximating $u''(t+\theta\Delta t)$ with $u''(t)$ on the right hand side, i.e.,

$$u(t+\Delta t) - 2u(t) + u(t-\Delta t) \approx \Delta t^2 u''(t).$$

Extension to high order version can be derived by the modified equation approach, as shown in [22, 42]. To obtain a fourth-order time discretization, we consider the Taylor expansion of $u''(t+\theta\Delta t)$ and the first three terms are:

$$u''(t+\theta\Delta t) \approx u''(t) + \theta\Delta t u'''(t) + \frac{\theta^2\Delta t^2}{2} u^{(4)}(t).$$

Inserting the above approximation into Eq. (4.9), the integral of odd powers of θ vanishes, and we have

$$u(t+\Delta t) - 2u(t) + u(t-\Delta t) \approx \Delta t^2 \left(u''(t) + \frac{\Delta t^2}{12} u^{(4)}(t) \right). \tag{4.10}$$

We comment here that if one considers a time integrator more accurate than fourth order, more terms should be included in the Taylor expansion. Applying (4.10) to the differential system (4.1), and utilizing the fact that $\boldsymbol{u}_h^{(4)}(t) = M^{-1}A\ddot{\boldsymbol{u}}_h(t) = (M^{-1}A)^2\boldsymbol{u}_h(t)$, one has the fourth-order method:

$$\frac{\boldsymbol{u}_h^{n+1} - 2\boldsymbol{u}_h^n + \boldsymbol{u}_h^{n-1}}{\Delta t^2} = M^{-1}A\boldsymbol{u}_h^n + \frac{\Delta t^2}{12}(M^{-1}A)^2\boldsymbol{u}_h^n, \tag{4.11}$$

It has been shown that the largest time step of this fourth-order method is $\sqrt{3}$ of that of the leap-frog method [21, 43], and therefore the computational cost is comparable yet the accuracy is improved. In our numerical simulations, we use Eq. (4.11) as the fourth-order time integrator.

We remark here that the same fourth-order method has been reformulated into a predictor-corrector method in [43]: for $n = 1, \ldots, N-1$, $u_h^{n+1} \in V_h^k$ is given by

$$M\frac{\boldsymbol{u}_h^* - 2\boldsymbol{u}_h^n + \boldsymbol{u}_h^{n-1}}{\Delta t^2} = A\boldsymbol{u}_h^n, \tag{4.12}$$

$$M\boldsymbol{u}_h^{n+1} = M\boldsymbol{u}_h^* + \frac{\Delta t^4}{12} A\mathbf{v}_h, \quad \mathbf{v}_h = \frac{\boldsymbol{u}_h^* - 2\boldsymbol{u}_h^n + \boldsymbol{u}_h^{n-1}}{\Delta t^2}, \tag{4.13}$$

based on the system (4.1). More precisely, it can be rewritten in the form of a second-order predictor step

$$\left(\frac{u_h^* - 2u_h^n + u_h^{n-1}}{\Delta t^2}, \psi\right)_K + (a\boldsymbol{q}_h^n, \nabla\psi)_K - (a^+(\boldsymbol{q}^n)_h^+ \cdot \boldsymbol{\nu}, \psi)_{\partial K} = 0, \tag{4.14}$$

$$(\boldsymbol{q}_h^n, \boldsymbol{\phi})_K + (au_h^n, \nabla\cdot\boldsymbol{\phi})_K - ((u_h^n)^-, a\boldsymbol{\phi}\cdot\boldsymbol{\nu})_{\partial K} = -(u_h^n\nabla a, \boldsymbol{\phi})_K, \tag{4.15}$$

and the corrector step

$$v_h = \frac{u_h^* - 2u_h^n + u_h^{n-1}}{\Delta t^2}, \tag{4.16}$$

$$(\boldsymbol{w}_h, \boldsymbol{\phi})_K + (av_h, \nabla\cdot\boldsymbol{\phi})_K - ((v_h)^-, a\boldsymbol{\phi}\cdot\boldsymbol{\nu})_{\partial K} = -(v_h\nabla a, \boldsymbol{\phi})_K, \tag{4.17}$$

$$(u_h^{n+1}, \psi)_K = (u^*, \psi)_K + \frac{\Delta t^4}{12}(a\boldsymbol{w}_h, \nabla\psi)_K - \frac{\Delta t^4}{12}(a^+(\boldsymbol{w})_h^+ \cdot \boldsymbol{\nu}, \psi)_{\partial K} = 0, \tag{4.18}$$

for all test functions $\psi \in V_h^k$ and $\boldsymbol{\phi} \in \Sigma_h^k$.

5 Numerical experiments

5.1 Example 1: Wave equation with a constant coefficient – a standing wave

5.1.1 Accuracy test in Q^k space

We consider the 2D wave equation with a constant coefficient, which is taken to be 1,

$$u_{tt} = \nabla^2 u, \quad (x, y) \in [0, 2] \times [0, 2], \tag{5.1}$$

with initial condition

$$u(x, y, 0) = \sin(\pi x)\sin(\pi y), \quad u_t(x, y, 0) = 0,$$

and periodic boundary conditions $u(0, y, t) = u(2, y, t)$ and $u(x, 0, t) = u(x, 2, t)$, for all $0 \le x \le 2, 0 \le y \le 2$ and $t \ge 0$.

This problem has the exact solution, which is a standing wave

$$u(x, y, t) = \cos(\sqrt{2}\pi t)\sin(\pi x)\sin(\pi y).$$

Table 5.1: Example 1 with Q^1 space: numerical errors and orders with uniform meshes.

N	error of u		error of u_x		error of u_y	
	L^2 error	order	L^2 error	order	L^2 error	order
10	4.9405E-03		1.3059E-02		1.3059E-02	
20	1.2323E-03	2.0033	6.7050E-03	0.9617	6.7050E-03	0.9617
40	3.1303E-04	1.9770	2.2976E-03	1.5451	2.2976E-03	1.5451
80	7.7676E-05	2.0108	3.7983E-04	2.5967	3.7983E-04	2.5967
160	1.9396E-05	2.0017	7.5453E-05	2.3317	7.5453E-05	2.3317

We implemented the LDG method with the alternating fluxes (2.17) and use the time integrator (4.11) with time step $\Delta t = 0.2/(\Delta x^{\frac{-5}{4}} + \Delta y^{\frac{-5}{4}})$. Since the symplectic time integrator requires initial conditions for two time steps, we consider Taylor expansion of u at $t = 0$:

$$u(x, y, \Delta t) = u(x, y, 0) + \Delta t u_t(x, y, 0) + \frac{\Delta t^2}{2} u_{tt}(x, y, 0) + \frac{\Delta t^3}{6} u_{ttt}(x, y, 0) + O(\Delta t^4),$$

and convert the higher derivatives of t to derivatives of x and y by repeatedly using the wave equation, while u and u_t are given by the initial conditions. To obtain the desired order of convergence of u, following the initial conditions (3.10), we take the projection P_h^+ of $u(x, y, 0)$, and L^2 projection P_h of $u_t(x, y, 0)$. In other words, with $u(x, y, 0)$ denoted by u_0 and $u_t(x, y, 0)$ by v_0, we use the initial conditions:

$$u_h^0 = P_h^- u_0, \tag{5.2}$$

$$u_h^1 = u_h^0 + \Delta t P_h v_0 + \frac{\Delta t^2}{2} P_h^-\{(\partial_{xx} + \partial_{yy})u_0\} + \frac{\Delta t^3}{6} P_h\{(\partial_{xx} + \partial_{yy})v_0\}. \tag{5.3}$$

Tables 5.1 – 5.3 list the numerical errors and the orders of convergence for Q^k spaces, $k = 1, 2, 3$. In each table, the L^2-norm of the errors e_u, e_p, and e_q at the final time $T = 1$ are presented. The $(k+1)$th order for all the errors of u, p, q can be observed clearly.

5.1.2 Accuracy test in Q^k space with standard L^2 projections for initial conditions

To show that the special projections of the initial condition u_0 in (5.2) is indeed critical for optimal rate of convergence, we test the problem with the same setting, but with standard L^2 projections for both u_0 and v_0. Tables 5.4 – 5.5 list the numerical errors and the orders

Table 5.2: Example 1 with Q^2 space: numerical errors and orders with uniform meshes.

N	error of u		error of u_x		error of u_y	
	L^2 error	order	L^2 error	order	L^2 error	order
10	2.7279E-04		1.7387E-03		1.7387E-03	
20	3.2450E-05	3.0715	1.7662E-04	3.2993	1.7662E-04	3.2993
40	4.1196E-06	2.9776	2.5073E-05	2.8164	2.5073E-05	2.8164
80	5.1406E-07	3.0025	2.5418E-06	3.3022	2.5418E-06	3.3022
160	6.4271E-08	2.9997	3.4971E-07	2.8616	3.4971E-07	2.8616

Table 5.3: Example 1 with Q^3 space: numerical errors and orders with uniform meshes.

N	error of u		error of u_x		error of u_y	
	L^2 error	order	L^2 error	order	L^2 error	order
10	1.2053E-05		5.3347E-05		5.3347E-05	
20	7.8368E-07	3.9430	4.0172E-06	3.7311	4.0172E-06	3.7311
40	5.0864E-08	3.9455	2.2137E-07	4.1817	2.2137E-07	4.1817
80	3.3455E-09	3.9264	1.2105E-08	4.1928	1.2105E-08	4.1928

of convergence for Q^1 and Q^2 spaces. We can observe that the order of accuracy for u, u_x and u_y is oscillating. When Q^2 space is used, the accuracy of u_x and u_y is close to 2, which means only suboptimal convergence rate is obtained. This oscillating behavior of numerical accuracy is commonly observed for energy conserving methods, and a least square fitting of the order [44] may give the optimal convergence rate of u. We notice that in Subsection 5.1.1, different initial conditions are employed and optimal convergence rates are clearly observed there. Previous studies on LDG methods showed that different choices of initial conditions have little impact on the convergence/superconvergence results [11, 37, 32]. This test demonstrates that our energy conserving method is more sensitive to the error in the initial conditions, probably due to the fact that no numerical dissipation is included in these methods to dissipate the initial error.

5.1.3 Accuracy test in P^k space

We consider the same problem and setup, but replace the DG spaces by P^k, which is the polynomial space that has degree at most k, namely, $\{\sum_{i,j} x^i y^j : i, j \in N, i + j \leq k\}$. According to extensive numerical experiments in previous works, $(k+1)$-th order accuracy

Table 5.4: Example 1 with Q^1 space and L^2 projections of the initial conditions: numerical errors and orders with uniform meshes.

N	error of u		error of u_x		error of u_y	
	L^2 error	order	L^2 error	order	L^2 error	order
10	2.8467e-03		1.0048e-01		1.0048e-01	
20	2.4944e-03	0.1906	1.4448e-01	-0.5240	1.4448e-01	-0.5240
40	1.0608e-03	1.2335	6.6667e-02	1.1158	6.6667e-02	1.1158
80	1.7083e-04	2.6345	1.7039e-02	1.9681	1.7039e-02	1.9681
160	2.3920e-05	2.8363	1.2683e-02	0.4259	1.2683e-02	0.4259
160	6.5615e-06	1.8661	1.3186e-03	3.2658	1.3186e-03	3.2658

Table 5.5: Example 1 with Q^2 space and L^2 projections of the initial conditions: numerical errors and orders with uniform meshes.

N	error of u		error of u_x		error of u_y	
	L^2 error	order	L^2 error	order	L^2 error	order
10	7.7825e-04		1.7934e-02		1.7934e-02	
20	7.0800e-05	3.4584	4.7146e-03	1.9275	4.7146e-03	1.9275
40	1.1093e-05	2.6741	1.0602e-03	2.1528	1.0602e-03	2.1528
80	9.9096e-07	3.4847	2.4853e-04	2.0928	2.4853e-04	2.0928
160	1.4768e-07	2.7464	7.0811e-05	1.8114	7.0811e-05	1.8114

can usually be observed for the P^k space. Since the space P^k is smaller than Q^k, using P^k will be more efficient in order to obtain $(k+1)$-th order accuracy. However, theoretically it is very difficult to prove the optimal order of accuracy for P^k space, and therefore in this paper, we only perform numerical experiments. As for the initial conditions, we simply project the initial conditions (5.2)-(5.3), which is defined in Q^k, to space P^k.

The orders of accuracy with spaces P^1, P^2 and P^3 are shown in Tables 5.6 – 5.8. For P^1, second order accuracy can be observed in all the variables u, p and q. However, for P^2 and P^3, $(k+1)$-th order can be achieved in u, but only k-th order of accuracy is seen in p and q. This loss of accuracy in p and q may be resulted from the initial projection (5.2)-(5.3), which has been shown essential for the Q^k space, but appears not to produce the same optimal order of accuracy for the P^k space.

Table 5.6: Example 1 with P^1 space: numerical errors and orders with uniform meshes.

N	error of u		error of u_x		error of u_y	
	L^2 error	order	L^2 error	order	L^2 error	order
10	1.2736e-02		6.3328e-02		6.3328e-02	
20	3.1285e-03	2.0254	1.8352e-02	1.7869	1.8352e-02	1.7869
40	7.8996e-04	1.9856	5.6663e-03	1.6955	5.6663e-03	1.6955
80	1.9682e-04	2.0049	1.1306e-03	2.3253	1.1306e-03	2.3253
160	4.9184e-05	2.0006	2.5818e-04	2.1306	2.5818e-04	2.1306

Table 5.7: Example 1 with P^2 space: numerical errors and orders with uniform meshes.

N	error of u		error of u_x		error of u_y	
	L^2 error	order	L^2 error	order	L^2 error	order
10	2.6763e-03		7.6128e-02		7.6128e-02	
20	2.0342e-04	3.7177	1.2275e-02	2.6327	1.2275e-02	2.6327
40	4.7780e-05	2.0900	4.2500e-03	1.5302	4.2500e-03	1.5302
80	6.3518e-06	2.9112	1.1668e-03	1.8649	1.1668e-03	1.8649
160	8.0589e-07	2.9785	2.9819e-04	1.9683	2.9819e-04	1.9683

Table 5.8: Example 1 with P^3 space: numerical errors and orders with uniform meshes.

N	error of u		error of u_x		error of u_y	
	L^2 error	order	L^2 error	order	L^2 error	order
10	1.5827e-04		3.9745e-03		3.9745e-03	
20	1.2081e-05	3.7116	8.3389e-04	2.2528	8.3389e-04	2.2528
40	8.6623e-07	3.8018	7.7308e-05	3.4312	7.7308e-05	3.4312
80	3.0307e-08	4.8370	1.2469e-05	2.6323	1.2469e-05	2.6323
160	2.0657e-09	3.8749	1.1613e-06	3.4245	1.1613e-06	3.4245

Table 5.9: Example 1 with Q^k and central flux: numerical errors and orders for u with uniform meshes, for Q^1, Q^2 and Q^3.

N	Q^1		Q^2		Q^3	
	L^2 error	order	L^2 error	order	L^2 error	order
10	2.8446e-02		1.9582e-04		7.5838e-05	
20	1.1325e-02	1.3287	1.8994e-05	3.3659	6.0140e-06	3.6565
40	5.1048e-03	1.1496	2.5060e-06	2.9221	8.1456e-07	2.8842
80	2.4699e-03	1.0474	2.9755e-07	3.0742	1.0012e-07	3.0243
160	1.2234e-03	1.0136	3.7259e-08	2.9975	1.2413e-08	3.0118

5.1.4 Accuracy test with central flux in the Q^k space

While claiming that the advantage of using alternating flux as proposed in this paper is to conserve energy, it is arguable that in (2.6), (2.15) and (2.16) using the central flux

$$\widehat{aq_h^1} = \{\{aq_h\}\}, \quad \widehat{u_h} = \{\{u_h\}\},$$

and

$$\widetilde{aq_h^2} = \{\{aq_h\}\}, \quad \widetilde{u_h} = \{\{u_h\}\},$$

where $\{\{u\}\} = \frac{u^- + u^+}{2}$, may also conserve energy, as is known when applied for first order hyperbolic equations. However, a well-known disadvantage of central flux is its order of accuracy oscillates, depending on if k is even or odd. Here we implement the LDG scheme, with central flux and show that the order of accuracy indeed oscillates (Table 5.9): the order for even k is $k+1$ and the order for odd k is k. Therefore it is not an optimal energy preserving method to use for any desired order of accuracy.

5.1.5 Time history of the L^2 error

To demonstrate that the growth of the L^2 error of our proposed method is at most linear, as proved in Section 3, we simulate the problem in Example 1 until $T = 100$ and monitor the L^2 error. When a 40×40 uniform mesh is used, it can be seen in Fig. 5.1 (upper panel) that the L^2 error stays at the level of 10^{-5} for Q^2 and 10^{-7} for Q^3, and the average values do not grow noticeably in time. As we reduce the resolution by using a 5×5 uniform mesh, the growth of errors can be seen to be bounded linearly. We also simulated with the central

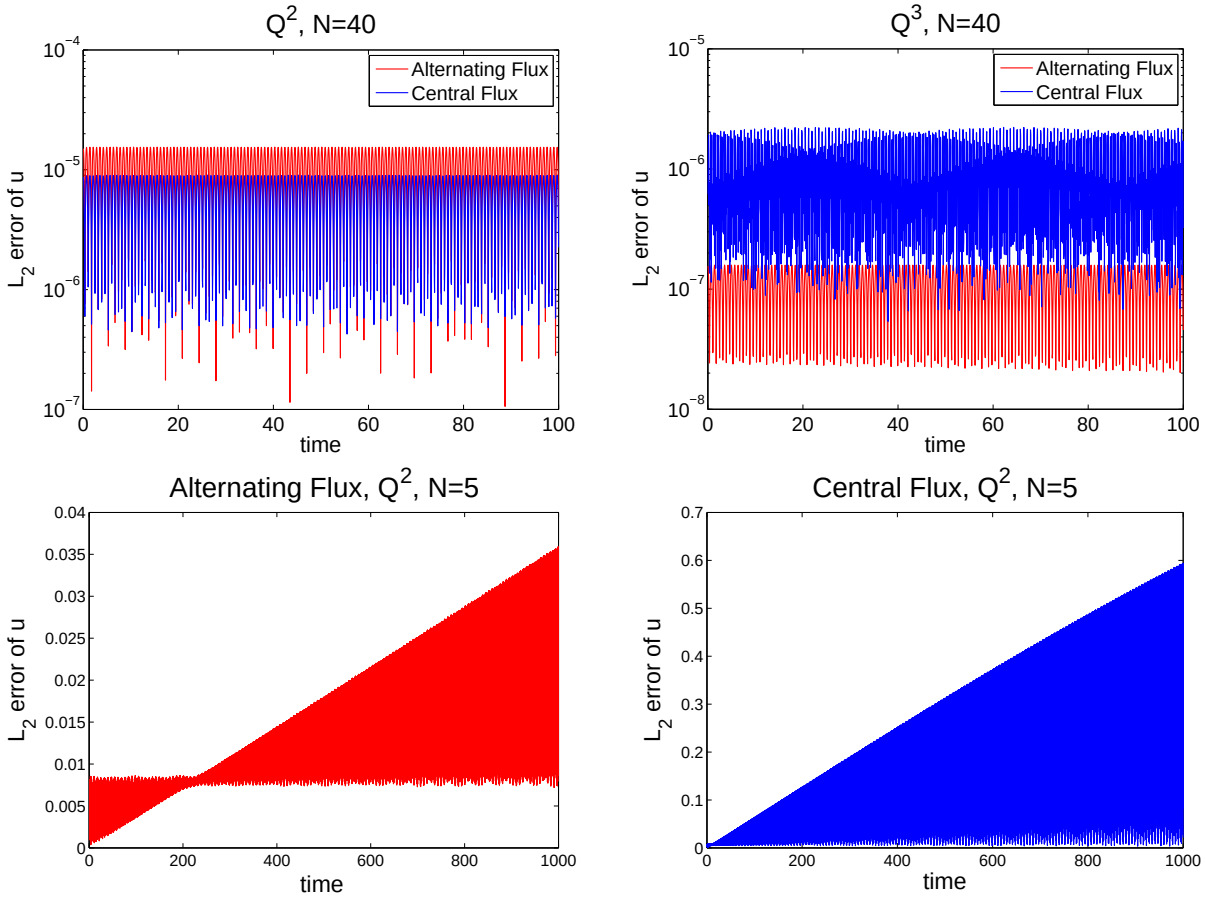

Figure 5.1: Example 1 with Q^k space. Upper panel: time history until $T = 100$ of the L^2 error of the numerical approximations obtained from using the alternating flux (red) and central flux (blue), with $k = 2, 3$. A uniform 40×40 grid is used. The L^2 error of u on y-axis are presented in log scale. Lower panel: A uniform 5×5 grid is used to observe the growth of errors until $T = 1000$. History of L^2 errors for central flux and alternating flux with Q^2 space are shown at left and right in linear scale, respectively.

flux for Q^2 and Q^3. Since the central flux also preserves energy, the L^2 error also remains roughly constant in average if a 40×40 uniform mesh is used. However, due to the nature of the oscillating order of accuracy, the L^2 error for Q^2 is comparable to that of alternating flux, but the error for Q^3 is much higher than using alternating flux. Moreover, if Q^2 space and a coarse 5×5 mesh are used, the growth of the errors for central flux is much faster than that for alternating flux (lower panel of Fig. 5.1).

5.2 Example 2: Wave equation with a constant coefficient – a traveling wave

In this example, we present a problem which has a traveling wave solution. This is to test whether the nice behavior of L^2 errors seen in Example 1 can still be observed in this traveling wave case. The equation is the same as Eq. (5.1), with periodic boundary conditions and initial conditions

$$u(x, y, 0) = \cos(\pi x)\cos(\pi y), \quad u_t(x, y, 0) = -\sqrt{2}\pi \sin(\pi x)\cos(\pi y),$$

and the exact solution is

$$u(x, y, t) = \cos(\sqrt{2}\pi t + \pi x)\cos(\pi y).$$

We tested spaces Q^2 and Q^3 with a well resolved 40×40 mesh, and the time history is displayed in the upper panel of Fig. 5.2. The figure shows that the L^2 errors stays constant in average over time. Similar to Example 1, as we decrease the resolution of the numerical solutions, the growth of the errors are more obvious. In the lower panel of Fig. 5.2, we use 5×5, 10×10 and 20×20 meshes, and it can be observed that the errors grow in a linear fashion asymptotically for the coarse meshes.

5.3 Example 3: Wave equation with discontinuous coefficient – standing wave

We consider the 2D wave equation

$$u_{tt} = \nabla \cdot (a^2(x, y)\nabla u), \tag{5.4}$$

with a discontinuous coefficient in the domain $\Omega = \{(x, y)|(x, y) \in [-2, 2] \times [-1, 1]\}$. The domain Ω is composed of two subdomains $\Omega_1 = [-1, 1] \times [-1, 1]$ and $\Omega_2 = \Omega \backslash \Omega_1$, and if the coefficient $a(x, y)$ is defined as

$$a(x, y) = \begin{cases} \sqrt{\frac{9}{34}}, & \text{in } \Omega_1 \\ \sqrt{\frac{1}{2}}, & \text{in } \Omega_2 \end{cases}$$

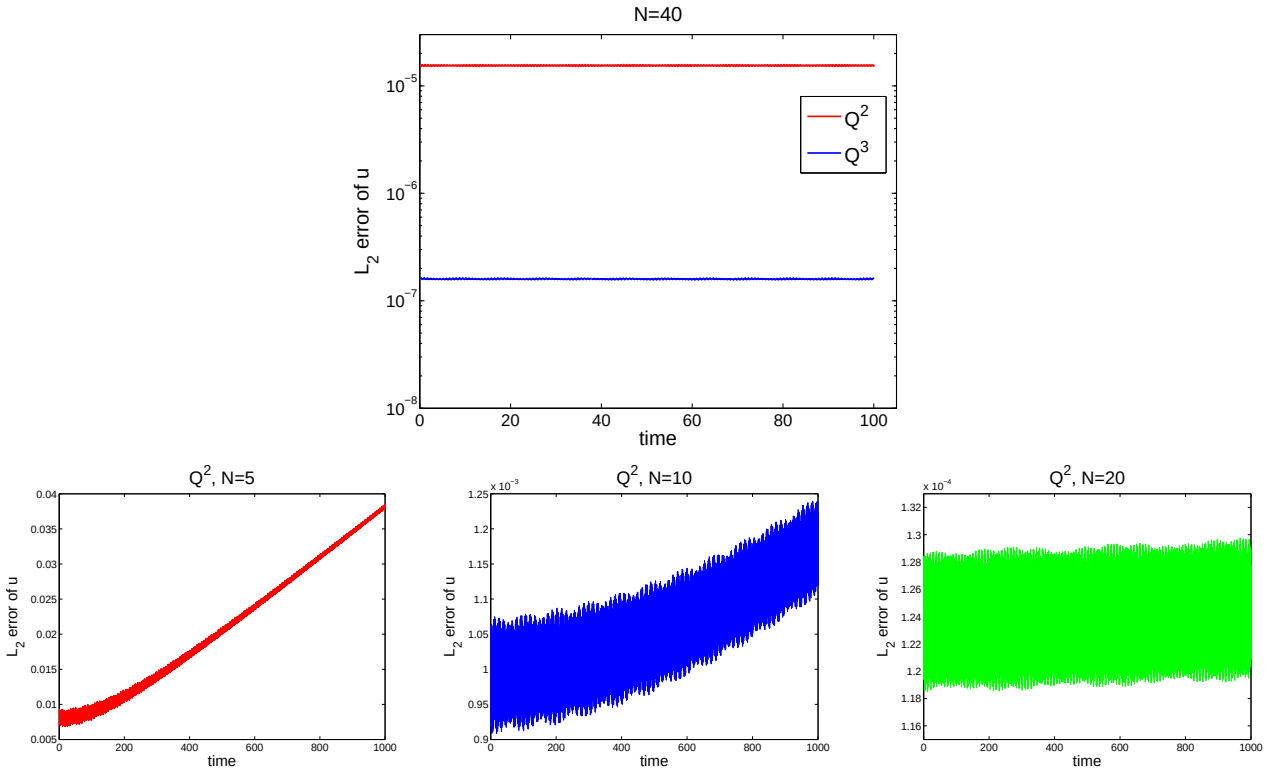

Figure 5.2: Example 2. Upper panel: time history until $T = 100$ of the L^2 error of the numerical approximations obtained from using the Q^2 (red) and Q^3 (blue) spaces. A uniform 40×40 grid is used. The L^2 error of u on y-axis are presented in log scale. Lower panel: time history until $T = 1000$ with Q^2 space, uniform meshes 5×5 (red), 10×10 (blue) and 20×20 (green) are used. The L^2 error of u on y-axis are presented in linear scale.

Table 5.10: Example 3: numerical errors and orders with uniform meshes and space Q^2.

$N_x \times N_y$	error of u		error of u_x		error of u_y	
	L^2 error	order	L^2 error	order	L^2 error	order
20×5	1.1173e-01		7.9322e-01		6.7706e-01	
40×10	1.4404e-02	2.9554	1.4475e-01	2.4541	1.6922e-01	2.0005
80×20	2.1081e-03	2.7725	2.4832e-02	3.1870	4.4012e-02	2.8145
160×40	2.3950e-04	3.1378	2.0700e-03	2.9408	2.0477e-03	3.5543
320×80	3.0262e-05	2.9844	3.3118e-04	2.6440	2.5500e-04	3.0054

and if we impose periodic boundary conditions in both x- and y-directions, then the solution is a standing wave

$$u(x,y,t) = \begin{cases} \cos(3\pi t)\cos(5\pi x)\cos(3\pi y), & \text{in } \Omega_1 \\ \cos(3\pi t)\cos(3\pi x)\cos(3\pi y), & \text{in } \Omega_2. \end{cases}$$

By using the alternating flux (2.17)-(2.18) designed for this type of problem, we present the order of accuracy Q^2 space in Table 5.10. Third order accuracy can be clearly seen in the all the variables. Spaces Q^1 and Q^3 were also tested, and we obtained second and fourth orders accuracy, respectively (data not shown).

5.4 Example 4: Wave equation with discontinuous coefficient – traveling wave

Here we test a problem with discontinuous coefficient but with a traveling wave solution. Consider Eq. (5.4) in the domain $\Omega = \{(x,y)|(x,y) \in [-2,2] \times [-1,1]\}$, and its two subdomains $\Omega_1 = [-1,1] \times [-1,1]$ and $\Omega_2 = \Omega \backslash \Omega_1$, where the coefficient is discontinuous at the interface:

$$a(x,y) = \begin{cases} \sqrt{\frac{4}{5}}, & \text{in } \Omega_1 \\ \sqrt{\frac{1}{5}}, & \text{in } \Omega_2. \end{cases}$$

If we impose periodic boundary conditions in both x- and y-directions, the solution is a traveling wave

$$u(x,y,t) = \begin{cases} \cos(4\pi t + 2\pi x)\cos(4\pi y), & \text{in } \Omega_1 \\ \cos(4\pi t + 8\pi x)\cos(4\pi y), & \text{in } \Omega_2. \end{cases}$$

In Fig. 5.3, we show the time history of the L^2 error until $T = 200$, using Q^2 and Q^3 spaces with 80×40 meshes. It can be observed that the L^2 errors grow linearly asymptotically on

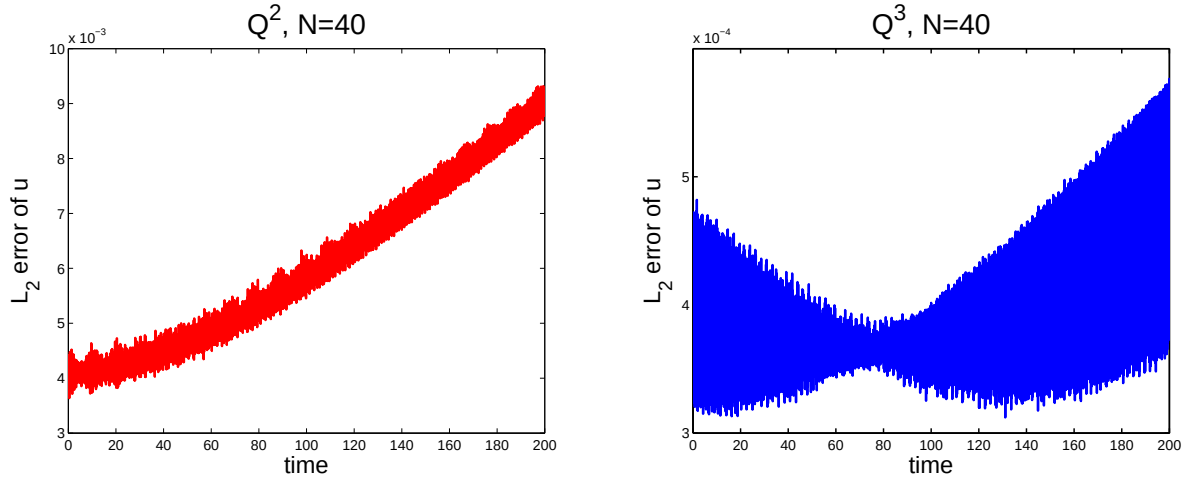

Figure 5.3: Example 4. Time history until $T = 200$ of the L^2 error of the numerical approximations obtained from using the Q^2 (red) and Q^3 (blue) spaces. A uniform 80×40 grid is used. The L^2 error of u on y-axis are presented in linear scale.

average, while the growth rate for Q^3 space is slower than that for Q^2 space. Oscillations in errors with Q^3 space appear larger than Q^2 space.

5.5 Example 5: Isotropic wave propagation within heterogeneous media

We consider the 2D wave equation Eq. (2.1) with discontinuous coefficient in the domain $[0, 1] \times [0, 1]$, with the coefficient $a(x, y)$ defined as

$$a(x, y) = \begin{cases} \frac{1}{2}, & \text{if } x \leq 0.65, \\ 1, & \text{if } x > 0.65. \end{cases}$$

The initial condition is given by

$$u(x, y, 0) = 0 \quad \text{and} \quad u_t(x, y, 0) = 2e^{-500((x-0.5)^2+(y-0.5)^2)}.$$

and zero boundary conditions are imposed for all the boundaries. Fig. 5.4 shows the time evolution of the wave propagation: initially the wave propagates isotropically, until it reaches the interface of two media (around $T = 0.25$ to 0.3), and at a later time, the wave fronts propagates at different speeds in these two media. To verify the convergence of our numerical solutions, we compared snapshots of the 2D contour at $T = 0.5$ with 40×40 and 80×80 cells, and the contours agree very well (Fig. 5.5). We further compared, for these two meshes,

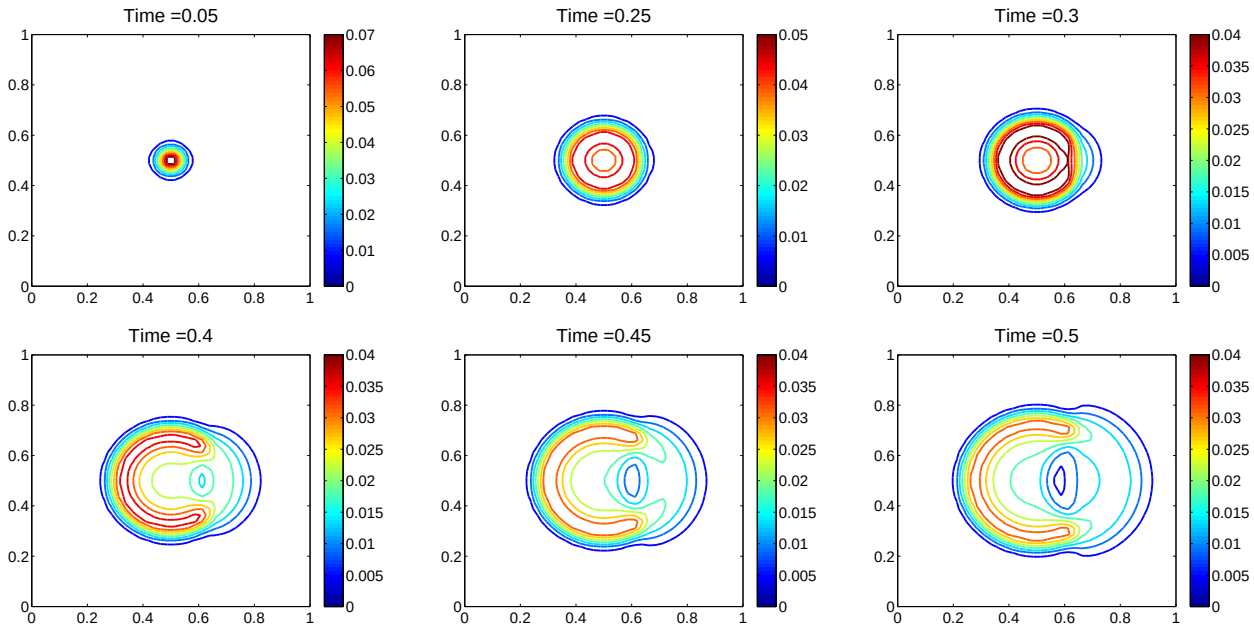

Figure 5.4: Example 5: Two-dimensional contours of the numerical approximations at time $T = 0.05, 0.25, 0.3, 0.4, 0.45, 0.5$. The DG space used is Q^2 and the grid is uniform with 40×40 cells.

the cross sections at $y = 0.4$ for $T = 0.05, 0.3, 0.5$. In Fig. 5.6, it can be seen that the one-dimensional profiles match very well.

6 Concluding remarks

In this paper, we have developed an LDG method for multi-dimensional wave problems in discontinuous media. As is well known, energy conservation is one of the most important properties of wave equations, and therefore this is the aimed property of our numerical method aside high order convergence rate. To obtain such a scheme, we carefully designed numerical fluxes and projections of the initial conditions. We also developed compatible time integrators, such as a second-order (leap-frog) and a fourth-order energy preserving method. We proved the optimal error estimate for the semi-discrete method, and also showed that our scheme preserves energy in the discrete sense. Numerous numerical examples were shown to demonstrate the optimal convergence rate and energy conservation property.

Future works include the generalization of the LDG scheme to wave equations, of which

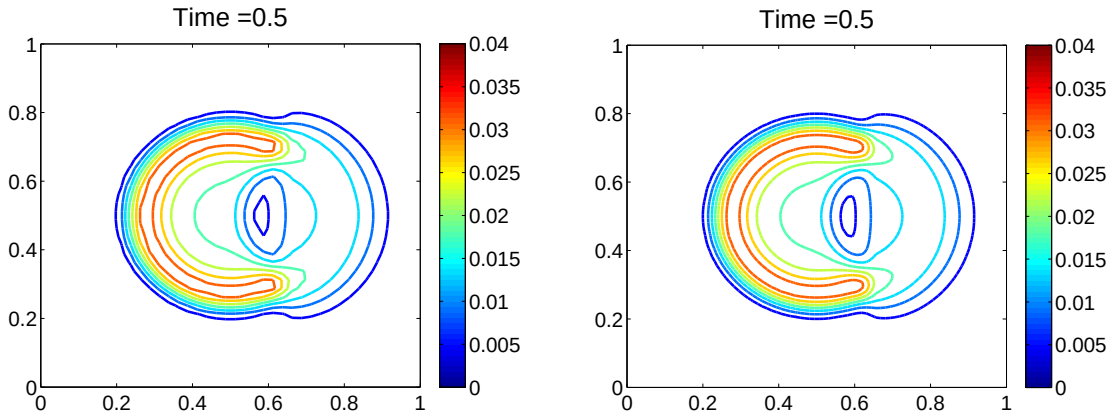

Figure 5.5: Example 5: Comparison of the 2D contours using 40×40 cells (left) and 80×80 cells (right), at $T = 0.5$.

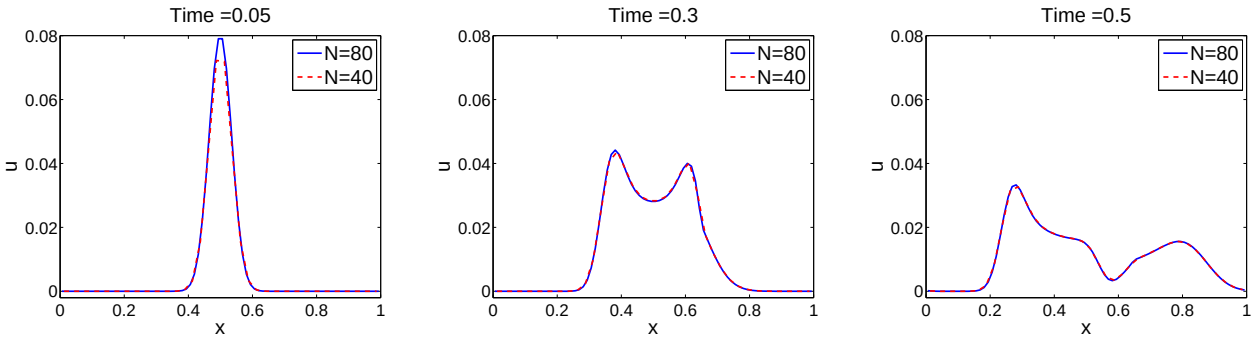

Figure 5.6: Example 5: Comparison of the cross sections of the numerical solutions at $y = 0.5$, at $T = 0.05, 0.3, 0.5$. The red dotted solutions are simulated with 40×40 cells, and the blue solid curves are for 80×80 cells.

the discontinuities of the coefficients are not aligned with the Cartesian grid. Schemes on unstructured triangular meshes will also be developed to accommodate general computational domains.

References

[1] S. Adjerid and H. Temimi. A discontinuous Galerkin method for the wave equation. *Computer Methods in Applied Mechanics and Engineering*, 200:837–849, 2011.

[2] M. Anderson and J.-H. Kimn. A numerical approach to space-time finite elements for the wave equation. *Journal of Computational Physics*, 226:466–476, 2007.

[3] D. Appelö, J. W. Banks, W. D. Henshaw and D. W. Schwendeman. Numerical methods for solid mechanics on overlapping grids: Linear elasticity. *Journal of Computational Physics*, 231:6012–6050, 2012.

[4] D. Appelö and N. A. Petersson. A stable finite difference method for the elastic wave equation on complex geometries with free surfaces. *Communications in Computational Physics*, 5:84–107, 2009.

[5] M. Baccouch. A local discontinuous Galerkin method for the second-order wave equation. *Computer Methods in Applied Mechanics and Engineering*, 209-212:129–143, 2012.

[6] J. W. Banks and W. D. Henshaw. Upwind schemes for the wave equation in second-order form. *Journal of Computational Physics*, 231:5854–5889, 2012.

[7] F. Bassi and S. Rebay. A high-order accurate discontinuous finite element method for the numerical solution of the compressible Navier-Stokes equations. *Journal of Computational Physics*, 131:267–279, 1997.

[8] D. L. Brown. A note on the numerical solution of the wave equation with piecewise smooth coefficients. *Mathematics of Computation*, 42:369–391, 1984.

[9] F. Casadei, E. Gabellini, G. Fotia, F. Maggio and A. Quarteroni. A mortar spectral/finite element method for complex 2d and 3d elastodynamic problems. *Computer Methods in Applied Mechanics and Engineering*, 191:5119–5148, 2002.

[10] Y. Cheng and C.-W. Shu. Superconvergence and time evolution of discontinuous Galerkin finite element solutions. *Journal of Computational Physics*, 227:9612–9627, 2008.

[11] Y. Cheng and C.-W. Shu. Superconvergence of discontinuous Galerkin and local discontinuous Galerkin schemes for linear hyperbolic and convection diffusion equations in one space dimension. *SIAM Journal on Numerical Analysis*, 47:4044–4072, 2010.

[12] E. T. Chung and B. Engquist. Optimal discontinuous Galerkin methods for wave propagation. *SIAM Journal on Numerical Analysis*, 44:2131–2158, 2006.

[13] E. T. Chung and B. Engquist. Optimal discontinuous Galerkin methods for the acoustic wave equation in higher dimensions. *SIAM Journal on Numerical Analysis*, 47:3820–3848, 2009.

[14] B. Cockburn, S. Hou, and C.-W. Shu. The Runge-Kutta local projection discontinuous Galerkin finite element method for conservation laws IV: the multidimensional case. *Mathematics of Computation*, 54:545–581, 1990.

[15] B. Cockburn, S.-Y. Lin, and C.-W. Shu. TVB Runge-Kutta local projection discontinuous Galerkin finite element method for conservation laws III: one dimensional systems. *Journal of Computational Physics*, 84:90–113, 1989.

[16] B. Cockburn and C.-W. Shu. TVB Runge-Kutta local projection discontinuous Galerkin finite element method for conservation laws II: general framework. *Mathematics of Computation*, 52:411–435, 1989.

[17] B. Cockburn and C.-W. Shu. The local discontinuous Galerkin method for time-dependent convection-diffusion systems. *SIAM Journal on Numerical Analysis*, 35:2440–2463, 1998.

[18] B. Cockburn and C.-W. Shu. The Runge-Kutta discontinuous Galerkin method for conservation laws V: multidimensional systems. *Journal of Computational Physics*, 141:199–224, 1998.

[19] B. Cockburn and C.-W. Shu. Runge-Kutta discontinuous Galerkin methods for convection-dominated problems. *Journal of Scientific Computing*, 16:173–261, 2001.

[20] G. Cohen. Higher-Order Numerical Methods for Transient Wave Equations. *Springer-Verlag*, Berlin, 2002.

[21] G. Cohen, P. Joly, J. Roberts and N. Tordjman. Higher order triangular finite elements with mass lumping for the wave equation. *SIAM Journal on Numerical Analysis*, 38:2047–2078, 2001.

[22] J. Diaz and M. J. Grote. Energy conserving explicit local time stepping for second-order wave equations. *SIAM Journal on Scientific Computing*, 31:1985–2014, 2009.

[23] B. Dong and C.-W. Shu. Analysis of a local discontinuous Galerkin method for linear time-dependent fourth-order problems. *SIAM Journal on Numerical Analysis*, 47:3240–3268, 2009.

[24] D. R. Durran. *Numerical Methods for Wave Equations in Geophysical Fluid Dynamics*. Springer, 1999.

[25] E. Faccioli, F. Maggio, A. Quarteroni and A. Tagliani. Spectral-domain decomposition for the solution of acoustic and elastic wave equations. *Geophysics*, 61:1160–1174, 1996.

[26] R. S. Falk and G. R. Richter. Explicit finite element methods for symmetric hyperbolic equations. *SIAM Journal on Numerical Analysis*, 36:935–952, 1999.

[27] L. Fezoui, S. Lanteri, S. Lohrengel and S. Piperno. Convergence and stability of a discontinuous Galerkin time-domain method for the 3D heterogeneous Maxwell equations on unstructured meshes. *Mathematical Modelling and Numerical Analysis (M^2AN)*, 39:1149–1176, 2005.

[28] D. A. French and T. E. Peterson. A continuous space-time finite element method for the wave equation. *Mathematics of Computation*, 65:491–506, 1996.

[29] D. Gottlieb and J.S. Hesthaven. Spectral methods for hyperbolic problems. *Journal of Computational and Applied Mathematics*, 128:83–131, 2001.

[30] M. J. Grote, A. Schneebeli and D. Schötzau. Discontinuous Galerkin finite element method for the wave equation. *SIAM Journal on Numerical Analysis*, 44:2408–2431, 2006.

[31] J. S. Hesthaven and T. Warburton. Nodal high-order methods on unstructured grids. I. Time-domain solution of Maxwell's equations. *Journal of Computational Physics*, 181:186–221, 2002.

[32] C. Hufford and Y. Xing. Superconvergence of the local discontinuous galerkin method for the linearized korteweg-de vries equation. *Journal of Computational and Applied Mathematics*, 255:441–455, 2014.

[33] N. A. Kampanis, J. Ekaterinaris and V. Dougalis. *Effective Computational Methods for Wave Propagation*. Chapman & Hall/CRC, 2008.

[34] C. Kane, J. E. Marsden, M. Ortiz and M. West. Variational integrators and the Newmark algorithm for conservative and dissipative mechanical systems. *International Journal for Numerical Methods in Engineering*, 49:1295–1325, 2000.

[35] H.-O. Kreiss and J. Oliger. Comparison of accurate methods for the integration of hyperbolic equations. *Tellus*, 24:199–215, 1972.

[36] F. Maggio and A. Quarteroni. Acoustic wave propagation by spectral methods. *East-West Journal of Numerical Mathematics*, 2:129–150, 1994.

[37] X. Meng, C.-W. Shu and B. Wu. Superconvergence of the local discontinuous Galerkin method for linear fourth order time dependent problems in one space dimension. *IMA Journal of Numerical Analysis*, 32:1294–1328, 2012.

[38] P. Monk and G. R. Richter. A discontinuous Galerkin method for linear symmetric hyperbolic systems in inhomogeneous media. *Journal of Scientific Computing*, 22-23:443–477, 2005.

[39] N. M. Newmark. A method of computation for structural dynamics. *Journal of the Engineering Mechanics Division*, 85:67–94, 1959.

[40] B. Riviere and M. F. Wheeler. Discontinuous finite element methods for acoustic and elastic wave problems. *Contemporary Mathematics*, 329:271–282, 2003.

[41] A. Safjan and J. T. Oden. High-order Taylor-Galerkin and adaptive hp methods for second-order hyperbolic systems: application to elastodynamics. *Computer Methods in Applied Mechanics and Engineering*, 103:187–230, 1993.

[42] G. R. Shubin and J. B. Bell. A modified equation approach to constructing fourth order methods for acoustic wave propagation. *SIAM Journal on Scientific and Statistical Computing*, 8:135–151, 1987.

[43] B. Sjögreen and N. Anders Petersson. A fourth order accurate finite difference scheme for the elastic wave equation in second order formulation. *Journal of Scientific Computing*, 52:17–48, 2011.

[44] Y. Xing, C.-S. Chou and C.-W. Shu. Energy conserving local discontinuous Galerkin methods for wave propagation problems. *Inverse Problems and Imaging*, 7:967–986, 2013.

[45] Y. Xu and C.-W. Shu. Optimal error estimates of the semi-discrete local discontinuous Galerkin methods for high order wave equations. *SIAM Journal on Numerical Analysis*, 50:79–104, 2012.

[46] E. Zampieri and L.F. Pavarino. An explicit second order spectral element method for acoustic waves. *Advances in Computational Mathematics*, 25:381–401, 2006.

[47] X. Zhong and C.-W. Shu. Numerical resolution of discontinuous Galerkin methods for time dependent wave equations. *Computer Methods in Applied Mechanics and Engineering*, 200:2814–2827, 2011.